This is to certify that the

dissertation entitled

Three-dimensional Rough Surface Growth:
A Radial Continuum Equation and a Discrete
Off-lattice Eden Cluster Growth Model

presented by

Eric William Kuennen

has been accepted towards fulfillment
of the requirements for

Ph.D. degree in Mathematics

Major professor

Date 11-09-01

# THREE-DIMENSIONAL ROUGH SURFACE GROWTH: A RADIAL CONTINUUM EQUATION AND A DISCRETE OFF-LATTICE EDEN CLUSTER GROWTH MODEL

By

Eric William Kuennen

A DISSERTATION

Submitted to
Michigan State University
in partial fulfillment of the requirements
for the degree of

DOCTOR OF PHILOSOPHY

Department of Mathematics

2001

ABSTRACT

THREE-DIMENSIONAL ROUGH SURFACE GROWTH: A RADIAL CONTINUUM EQUATION AND A DISCRETE OFF-LATTICE EDEN CLUSTER GROWTH MODEL

By

Eric William Kuennen

The study of the propagation of rough surfaces has a rich variety of applications in physics and biology including fluid flow, vapor and electron deposition, tumor and bacterial growth, and epidemiology. A stochastic partial differential equation for three-dimensional surface growth in the radial geometry is proposed. The equation reduces to the KPZ equation in the large radius limit. The equation is analyzed numerically and the growth exponent is estimated. Two distinct scaling regimes are discovered. Further, a three-dimensional, off-lattice Eden-C cluster growth model is proposed. The discrete model grows compact clusters of non-overlapping, contiguous spherical cells. A proof that Eden clusters are compact is extended to off-lattice clusters. Large-scale computer simulations show that the model creates isotropic clusters, with interior volume density constant at approximately 0.43. The clusters have a self-affine surface, which propagates with a growth exponent $\beta \approx 0.12$. These results are used to discuss whether the radial continuum equation and three-dimensional off-lattice Eden growth belong to the KPZ universality class.

## ACKNOWLEDGMENTS

I would like to thank my advisor C. Y. Wang for his patience, encouragement and support; Clifford Weil for his careful reading and proofing of the manuscript; Chi Chia Chu, Zhengfang Zhou and Baisheng Yan their great kindness; Barbara Miller; the Mathematics and Computer Science Department at Ripon College, especially Norm Loomer; Simmons College, especially David Browder, Bob Goldman, Micheal Brown, Nanette Veilleux, and Donna Beers; Northeastern University for use of their research computers; Richard Moeckel at the University of Minnesota for cultivating my interest in mathematics; my good friend Fery; Scott and Michele for their hospitality on my many trips back to East Lansing; my parents; and most of all my wife Marianne, for without her I would not have completed or even thought to persue a doctorate in mathematics.

## TABLE OF CONTENTS

# LIST OF TABLES

## LIST OF FIGURES

# Chapter 1

# Introduction

A large variety of physical and biological processes are associated with growing interfaces and the propagation of rough surfaces, such as fluid flow in a porous medium, directed polymers in a random medium, colloid aggregation, atomic deposition, bacterial growth and tumor growth. Of recent technological interest is the applications to molecular-beam epitaxy and to the detection of cancerous cell growth. These seemingly very different phenomena each result in very complex structures with intricate growth behaviors, yet there seems to be strong universalities underlying and connecting these growth processes. A precise knowledge of growth mechanisms that govern these process, as well as the equivalence among various growth processes is naturally of great interest.

A rich theory of self-affine scaling has been developed to describe the behavior of these growth processes, and both discrete and continuous mathematical models for rough surface growth have been proposed and studied. The most widely studied models are the KPZ stochastic differential equation and the discrete Eden cluster growth model, and these models have been very successful in describing a large class of many kinds of one-dimensional surfaces and interfaces. However, the behavior of these models for two-dimensions is less well understood and a matter of some controversy, and thus is the focus of this study. In particular, we will study the effect

of modeling surface growth radially from a seed, as opposed to vertically from a flat substrate which is the standard geometry used, and the effect of not using a lattice in the discrete Eden model.

## 1.1 Fractals and Cluster Growth Models

The middle thirds Cantor set and the Sierpinski gasket are well-known examples of mathematical, or deterministic fractals. These objects are self-similar under an isotropic rescaling of lengths. That is, the set can be divided into $k$ congruent subsets that each can be magnified by a constant factor to produce the entire set. The standard process of producing these objects is to start with an ordinary (non-fractal) set and iteratively remove parts of the set in a regular, deterministic fashion. As the process continues, the remaining connected parts of the set get smaller in size. The result after an infinite number of iterations is a bounded set, and in the case of the Cantor set, a totally disconnected set.

The best-known measure of a fractal set is its *fractal dimension.* It is derived from the concept of volume of ordinary objects. Let $N(l)$ be the number of $d$-dimensional boxes, with volume $l^d$ needed to cover an ordinary $d$-dimensional object. Then it is natural to define the volume as

$$V = \lim_{l \to 0} N(l) l^d.$$

Hence $N(l)$ is proportional to $l^{-d}$ as $l \to 0$. Then for any object, if

$$N(l) \sim l^{-D} \text{ as } l \to 0,$$

then $D$ is defined as its fractal dimension. This is the exponent that describes how the number of remaining connected parts scales with their size.

Cluster growth models produce sets that are not mathematical fractals, but similar to them in many respects. They are called growing, or random fractals, because they differ from mathematical fractals in that the size of the object grows as time goes on, and the process is random, rather than deterministic. Growing fractals are typically self-similar only in the statistical sense: averaged quantities, such as the number or location of points, will be the same under a finite rescaling of lengths. Often the statistical self-similarity is valid under an *anisotropic* rescaling; that is, scaling by a different power in different directions. In this case the object is referred to as *self-affine.* The process for producing these objects is to put together particles of some fixed size. Starting from the seed particle, new particles are added to the cluster according to some stochastic growth rule. As the process continues, the particles remain fixed in size, but the set grows in size without bound with the addition of new particles.

The fractal dimension for growing fractals is defined analogously with mathematical fractals, by substituting $l = 1/L$, where $L$ now represents the linear size of the growing object. So the fractal dimension of a growing fractal is given by

$$N \sim L^D \text{ as } L \to \infty.$$

For example, the Diffusion Limited Aggregation model (DLA) grows clusters by letting a particle that is far from the cluster diffuse with a random walk until it lands on a site adjacent to the cluster, where it then sticks and joins the cluster. This model

produces clusters that are statistically self-similar and have a fractal dimension of approximately 1.7.

Describing the growth of cancerous tumors was an impetus for the study of growing fractals, and is still of current interest. Recent studies investigate the fractal dimension of the ragged boundary of cancerous cells and the DLA-like branching vascular patterns around them. [2]

## 1.2 The Eden Model

In 1961, Eden [13] introduced a discrete stochastic growth model for tumor growth, which has become a standard model for describing the propagation of rough surfaces in various applications such as epidemiology, percolation theory, vapor deposition, bacterial growth, propagation of flame fronts, and fluid flow in a porous media. The original model was 2-dimensional and used a square lattice. The basic idea was this: starting with seed particle at the origin, at each iteration a new particle, or cell, is added to the cluster at random at a neighboring empty site (lattice point). Julien and Botet [21] proposed three versions of the Eden model: (A) an unoccupied neighboring site is chosen at random; (B) a free bond between the cluster and then an unoccupied neighboring site is chosen at random; and (C) a surface site is chosen, then one of its unoccupied neighboring sites is chosen at random. Version C seems to have the fastest convergence to the scaling properties, and this is the method of the discrete model presented in Chapter 3. Note that versions A and B do not lend themselves well to off-lattice simulations, since there is not a finite list of open sites or free bonds

to choose from when working off a lattice.

Eden clusters themselves are not fractal objects, in fact, it has been shown that Eden clusters grown on a lattice are compact [11], and this is shown to be true for off-lattice clusters later in Chapter 3. What is of particular interest is the rough boundary or surface of Eden clusters, which are self-affine fractals [21]. In two dimensions, the exponents of the fractal scaling of the boundary are well-established, both numerically and theoretically. However, there has been no consensus on the fractal scaling of the boundary of three-dimensional clusters and there exists so far no accepted theoretical prediction. Three-dimensional Eden clusters are of special interest because of applications to cell clusters and the growth of tumors.

It is probable that some of the surface scaling properties (see next section) of 3-dimensional Eden clusters are affected by the anisotropy associated with on-lattice models. The Eden model is usually implemented on a lattice. Eden clusters grown on a lattice are anisotropic, as growth is preferred in the lattice directions, leading to a diamond shape as the size of the cluster gets large [4]. While the anisotropy is weak in terms of the overall shape of the cluster, about a 2% increase in the lattice directions, the effect on the surface width, a key property when measuring the scaling properties of the surface, has been shown to vary by about 10% [45]. A two-dimensional off-lattice Eden model has been introduced [43], but no 3-dimensional off-lattice version is known.

In Chapter 3 of this thesis, a three-dimensional off-lattice Eden cluster growth model is introduced. One theoretical algorithm is discussed, and two numerical algorithms are implemented to grow eden clusters in large-scale simulations. Several

properties of the model are discussed, including the density and the compactness of the clusters, and fractal scaling properties of the boundary, specifically the surface-width growth exponent $\beta$.

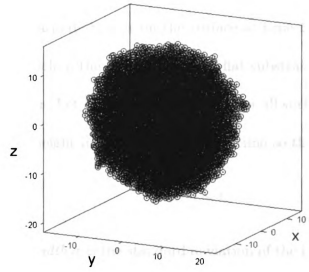


Figure 1.1: Typical three-dimensional off-lattice Eden cluster of 10000 Cells

## 1.3 Self-Affine Scaling of Surface Growth

The Eden Model for cluster growth, and hence for surface growth, is believed to be part of a universality class of models that produce surfaces with identical scaling exponents for the surface growth. When studying the growth or propagation of rough surfaces, such as the boundary of a growing Eden cluster, two exponents of interest are the roughness exponent $\alpha$ and the growing exponent $\beta$. Both exponents describe the behavior of the surface width, which measures the roughness of the surface. For

a more thorough discussion of what follows, please refer to the book by Barabási and Stanley [3] or Vicsek [41].

Surface width is defined as follows. We define the *surface* or cluster *boundary* $S$ as the set of all particles, or nodes $x$, that have an empty neighboring site for new growth. Let $x$ be a node that is on the surface at time $t$. Let $h(x,t)$ be the height of the surface particle if the growth is from a flat substrate, or the distance from the center of the cluster. Let $\overline{h}$ be the mean height over all surface sites. Time $t$ is defined so that the mean height increases linearly with time so that

$$\overline{h}(t) \sim t. \tag{1.1}$$

Then the *surface width* $\sigma$ is the standard deviation of the height over all surface sites,

$$\sigma^2 = \frac{1}{N}\sum_{x\in S}[h(x,t) - \overline{h}]^2, \tag{1.2}$$

where $N$ is the number of surface nodes in the cluster.

As the surface evolves with time, the surface width increases. Initially, width increases proportionally to time to the power $\beta$, called the *growth exponent.* That is,

$$\sigma \sim t^{\beta} \quad \text{for} \quad t \ll t_{\text{sat}}. \tag{1.3}$$

For a typical surface growth phenomenon with a finite system size, however, there is a saturation time $t_{\text{sat}}$ when the surface width approaches a constant saturation value $\sigma_{\text{sat}}$. Hence in a log-log plot of surface width $\sigma$ against time, there are two distinct scaling regimes, starting out linear with slope $\beta$, then leveling off after $t_{\text{sat}}$. For the same growth phenomenon, carried out in systems of different sizes, the saturation

width $\sigma_{\text{sat}}$ increases proportionally to the system size $L$ to the power $\alpha$, called the *roughness exponent.* That is,

$$\sigma_{\text{sat}} \sim L^{\alpha} \quad \text{for} \quad t \gg t_{\text{sat}}. \tag{1.4}$$

The time for saturation $t_{\text{sat}}$ scales with the system size with an exponent $z$, called the *dynamic exponent.* Hence,

$$t_{\text{sat}} \sim L^{z}. \tag{1.5}$$

Typically the system size $L$ for a surface growth model is based on a substrate that is a strip or hyperplane of length $L$ with periodic boundary conditions. The discrete and continuous models presented in the next two chapters use the radial geometry, with the height function replaced by a radial function which gives the radial distance from the center of mass. In this case, there is no finite system size and so there is not expected to be any surface width saturation. Hence the only exponent that is accessible is the growth exponent $\beta$.

Also, for general surface growth phenomenon described above, time is defined so that it varies linearly with the mean radius. So the growth exponent $\beta$ can be recovered by scaling surface width to mean height (or radius); that is

$$\sigma \sim \overline{h}^{\beta}. \tag{1.6}$$

The three scaling exponents are related, and this can be expressed by the scaling relation first introduced by Family and Vicsek [14],

$$\sigma(t, L) \sim L^{\alpha} f(\frac{t}{L^{z}}). \tag{1.7}$$

The scaling function $f(u)$ behaves in the following way:

$$f(u) = \begin{cases} u^{\beta}, & \text{if } u \ll 1 \\ \\ \text{constant}, & \text{if } u \gg 1 \end{cases}, \tag{1.8}$$

and results in the following scaling law linking the three exponents:

$$z = \frac{\alpha}{\beta}. \tag{1.9}$$

The self-affine nature of the scaling relation is seen by observing that the surface width scales by rescaling time $t$ by $L^{-z}$, and then rescaling the scaling function $f$ by $L^{\alpha}$.

The significance of the scaling exponents and the scaling relation is that they can be used to classify various surface growth models and phenomena. Different models and physical phenomena that have the same scaling exponents are said to belong to the same *universality class.*

For Eden clusters grown in two dimensions, the scaling exponents have been consistently found [20, 33, 47] to be $\alpha \approx \frac{1}{2}$, $\beta \approx \frac{1}{3}$, and $z \approx \frac{3}{2}$. This places the two-dimensional Eden model in the same universality class as other simulation models such as ballistic deposition and solid-on-solid, and the continuum KPZ equation, which is discussed in the next section.

In higher dimensions, there is no such consensus for the scaling exponents of Eden clusters. See Table 1.1 for a summary. The reasons for this are not certain. Computations in three dimensions are more cumbersome, and it maybe that crossover effects, finite size effects, or lattice effects may be more prominent in three dimensions. The purpose of the present study is to shed some light on this problem.

## 1.4 The KPZ Equation

To study the growth of an Eden surface analytically it is naturally desirable to be able to associate with the discrete growth process a continuum growth equation. Let $h(\mathbf{x}, t)$ be the height of the surface at position $\mathbf{x}$ at time $t$. We aim to write a partial differential equation for the time rate of change of the height, $\frac{\partial h}{\partial t}$. In order for the equation to be invariant under translations of time $t$, position $\mathbf{x}$, and in the growth direction $h$, the equation cannot be explicitly dependent on these quantities, and so will be constructed from combinations of the space derivatives $\nabla^n h$. Similarly, symmetry under the inversion $\mathbf{x} \to -\mathbf{x}$ excludes odd-order derivatives such as $\nabla h$. Thus, the simplest linear equation to describe a randomly growing surface is

$$\frac{\partial h(\mathbf{x}, t)}{\partial t} = \nu \nabla^2 h + \eta(\mathbf{x}, t), \tag{1.10}$$

called the Edward-Wilkinson equation [41, 3]. Here $\nu$ is called the *surface tension*, since the $\nu \nabla^2 h$ term has the effect of smoothing the surface. The stochastic nature of the growth process is represented by the random noise term $\eta(\mathbf{x}, t)$, which is usually assumed to be uncorrelated with a Gaussian distribution, so that

$$\langle \eta(\mathbf{x}, t) \rangle = 0, \quad \text{and} \quad \langle \eta(\mathbf{x}, t) \eta(\mathbf{x}', t') \rangle = 2D\delta^d(\mathbf{x} - \mathbf{x}')\delta(t - t'), \tag{1.11}$$

where $d$ is the surface dimension, and $D$ is a constant.

The Edward-Wilkinson equation can be solved explicitly, and the scaling exponents are

$$\alpha = \frac{2-d}{2}, \quad \beta = \frac{2-d}{4}, \quad z = 2. \tag{1.12}$$

Hence the Edward-Wilkinson equation does not describe Eden growth. To do this,

Kardar, Parisi, and Zhang in 1986 proposed to include the lowest-order non-linear term, resulting in what is known as the KPZ equation [22]:

$$\frac{\partial h(\mathbf{x},t)}{\partial t} = \nu\nabla^2 h + \frac{\lambda}{2}(\nabla h)^2 + \eta(\mathbf{x},t). \tag{1.13}$$

The non-linear term is required to allow lateral growth; that is, growth that is *locally* normal to the surface. The KPZ equation can be mapped to the Burgers equation for a vorticity-free velocity field, and to the diffusion equation for a directed polymer in a random environment. It is known that the inclusion of higher order non-linear terms, such as $\nabla^4 h$ will not affect the scaling properties.

The KPZ equation yields the Family-Vicsek scaling relation for surface propagation. The scaling law

$$\alpha + z = 2, \tag{1.14}$$

holds in all dimensions. This, together with the relation $\beta = \frac{\alpha}{z}$, implies that there is only one independent scaling exponent for KPZ surface growth.

The KPZ equation can be solved analytically in one dimension only. For one dimension, the existence of a fluctuation-dissipation theorem yields the following exact values for the scaling exponents:

$$\alpha = \frac{1}{2}, \quad \beta = \frac{1}{3}, \quad z = \frac{3}{2}. \tag{1.15}$$

A great many surface growth models share these same scaling exponents, including ballistic deposition, solid-on-solid models, and the surface of 2-dimensional Eden clusters. These models are said to all belong to the universality class described by the KPZ equation in one dimension. Of special interest is what the scaling exponents

are for the two-dimensional KPZ equation, and whether the two-dimensional surface of 3D Eden clusters belong to this universality class.

A common analytical approach to the KPZ equation is a renormalization-group analysis [35]. The focus is on the interaction or *coupling* of the three parameters in the KPZ equation: the surface tension $\nu$, the non-linear parameter $\lambda$ stemming from the growth velocity, and the noise parameter $D$. Renormalization group techniques show that for $d = 1$, there is an attracting fixed point for the parameters, resulting in a single scaling behavior yielding the exponents in Equation (1.15). For $d > 2$, there are two scaling regimes, a weak-coupling regime where the non-linearity $\lambda$ is insignificant and the scaling behavior is that of the linear Edwards-Wilkinson Equation (1.10), and a strong-coupling regime where the non-linearity is important, however the exponents have not yet been determined analytically.

In between is $d = 2$, which is the physically important dimension and the focus of this paper. Here there is no known fixed point for the coupling behavior. In the absence of the non-linearity $\lambda$, $d = 2$ is a critical dimension for the linear Edwards-Wilkinson exponents, see Equation (1.12), where $z = 2$, and $\alpha = \beta = 0$, so the surface width grows only logarithmically. This is likely to have an effect on the non-linear behavior with $d = 2$.

In the absence of analytical solutions for $d \geq 2$, there has been much focus on numerical integration. Numerical solutions have yielded differing results. In the first numerical study of the KPZ equation, Chakrabarti and Toral [8] in 1989 found $\beta \approx 0.10$ for $d = 2$. More recent studies by Colaiori and Moore [9, 10], and by Marinari, Pagnani and Parisi [31] give results closer to $\beta \approx 0.25$.

There is also much debate regarding the existence of an upper critical dimension, above which $z$ is 2, and hence both $\alpha$ and $\beta$ are zero. This would mean that the surface width grows only logarithmically. Colaiori and Moore claim that the critical dimension is $d = 4$, while others [31, 7] refute this by finding a positive value for $\alpha$ in $d = 4$. Honda and Matsuyama [19] show analytically that the critical dimension is $d = 2$, and that as a continuum model, the KPZ equation loses its mathematical basis for $d \geq 2$. Hence, the continuous KPZ equation and its discrete versions for numerical integration may very well have different scaling properties and this must be considered when placing the Eden model into a universality class.

| Summary of Values for Exponents for KPZ in $d = 2$ | | | | |
|---|---|---|---|---|
| **Source** | **Year** | **Type of Study** | $\alpha$ | $\beta$ |
| Chakrabarti, Toral | 1989 | Numerical | - | 0.10 |
| Guo, Grossmann, Grant | 1990 | Numerical | $.24 \pm .04$ | $.13 \pm .02$ |
| Moser, Kertesz, Wolf | 1991 | Numerical | - | 0.24 |
| Beccaria, Curci | 1994 | Numerical, Hopf-Cole | 0.404 | 0.240 |
| Marinari,Pagnani,Parisi | 2000 | Numerical | 0.4 | (0.25) |
| Castellano, etal | 1999 | Analytical, RG | 1/3 | 1/5 |
| Colaiori, Moore | 2001 | Analytical, mode-coupling | (0.38) | (0.23) |
| **Summary of Values for Exponents for 3D Eden Model ($d = 2$)** | | | | |
| **Source** | **Year** | **Type of Study** | $\alpha$ | $\beta$ |
| Julien, Botet | 1985 | Eden C | 0.20 | (0.11) |
| Wolf, Kertesz | 1987 | Noise Reduction | 0.33 | 0.22 |
| Devillard, Stanley | 1989 | Noise Reduction Eden B | 0.39 | .22 |

Table 1.1: Scaling Exponents in Three Dimensions, for Surfaces of Dimension $d = 2$. Parenthesis indicate that the value was not calculated directly, but results from another calculated exponent and the scaling relation $\alpha + \frac{\alpha}{\beta} = 2$.

# Chapter 2

# A Continuum Equation for Radial Surface Growth in Three Dimensions

The KPZ equation has been the standard continuum model for describing the propagation of rough surfaces. However, in the physically important case $d = 2$ for surfaces grown in three dimensions, previous analytical and numerical investigations of the equation have been inconclusive. The KPZ equation uses a flat substrate geometry, however many physical phenomena would be best modeled by radial growth from a single seed. To this end, a new continuum model for the propagation of a rough surface in a three-dimensional radial geometry will be proposed and discussed.

## 2.1 The Batchelor, Henry and Watt Equation

Batchelor, Henry and Watt [5] in 1998 introduced a stochastic differential equation (BHW), motivated by the KPZ equation, for $d = 1$ dimensional surface growth in a radial geometry from a single seed. This is the geometry used in the discrete off-lattice model presented in the next chapter. Like the KPZ equation, three terms are included: surface tension, lateral growth, and noise. Instead of the height function, we study the radial position function $R(\theta, t)$ at the polar angle $\theta$ and at time $t$. The

BHW equation is:

$$\frac{\partial R(\theta,t)}{\partial t} = \frac{v}{R}[R^2 + (\frac{\partial R}{\partial \theta})^2]^{\frac{1}{2}} - \nu\frac{R^2 + 2(\frac{\partial R}{\partial \theta})^2 - R\frac{\partial^2 R}{\partial \theta^2}}{[R^2 + (\frac{\partial R}{\partial \theta})^2]^{\frac{3}{2}}} + \eta(\theta,t). \qquad (2.1)$$

In their paper, Batchelor, Henry and Watt write their equation for $d = 1$ only consider that case. They analytically determine solutions in the deterministic (no noise) case, and numerically integrate the stochastic equation. They claim to recover the growth exponent $\beta \approx \frac{1}{3}$ for $d = 1$, but only for very large times. In the remainder of this section, the BHW equation for the case $d = 1$ will be analyzed further, to be followed by a new numerical integration in the next section.

### 2.1.1 The Reduced BHW Equation

The BHW equation is significantly more complicated in its presentation than the KPZ equation. While the geometrical considerations of surface tension and lateral growth motivated both equations, the KPZ equation has been simplified by using the small gradient approximation $\nabla h \ll 1$ and transforming to the co-moving frame so that the constant velocity term is zero.

Similar transformations will now be made and we will look at only the lower-order terms, noting as before that the inclusion of higher order terms will not affect the scaling properties.

First, a simplified derivation of the lateral growth term in the radial geometry will be shown. Figure 2.1 shows growth in the direction locally normal to the interface, which is not generally in the outward radial direction, and hence is termed lateral growth. Growth is shown with average velocity $v$ in the normal direction from a point

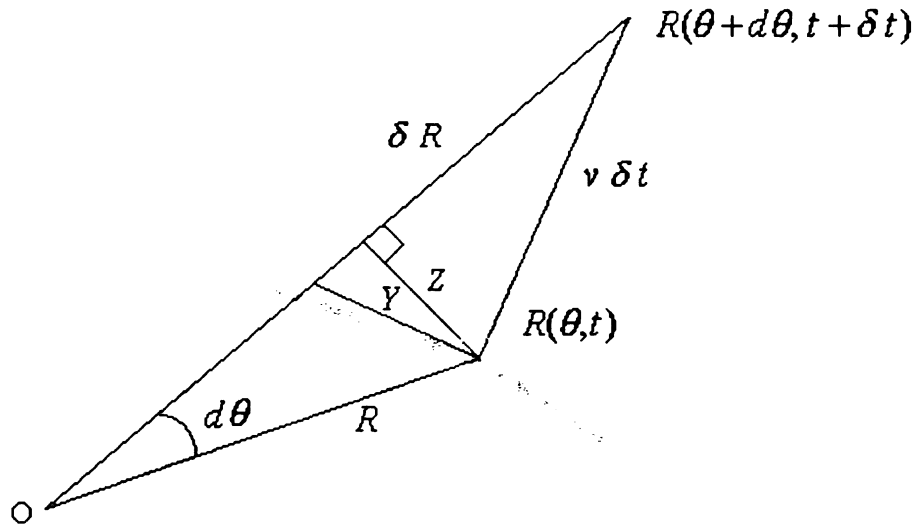


Figure 2.1: The derivation of the lateral growth term in the radial geometry. The surface interface is shown as the thick grey line.

$R(\theta, t)$ on the surface over a small time interval $\delta t$, with a corresponding change in the radius $\delta R$. Since this growth is lateral, it involves a change in the angular coordinate of $d\theta$. With time $t$ fixed, a change in the angle by $d\theta$ results in a change of the radius by $dR$ away from the local tangent plane.

First, notice that

$$Z = R\sin(d\theta) \approx Rd\theta. \tag{2.2}$$

Now by similar triangles, we have

$$\frac{v\delta t}{Y} = \frac{Rd\theta}{dR}, \tag{2.3}$$

$$Y = \frac{v\delta t}{R}\frac{dR}{d\theta}. \tag{2.4}$$

By the Pythagorean Theorem, we have

$$(\delta R)^2 = (v\delta t)^2 + (\frac{v\delta t}{R}\frac{dR}{d\theta})^2 \tag{2.5}$$

$$(\delta R)^2 = \frac{(v\delta t)^2}{R^2}[R^2 + (\frac{dR}{d\theta})^2]. \tag{2.6}$$

Finally, by letting $\delta t \to 0$, we have the lateral growth term for the component of the growth velocity in the locally normal direction as

$$\frac{\partial R}{\partial t} = \frac{v}{R}[R^2 + (\frac{\partial R}{\partial \theta})^2]^{\frac{1}{2}}. \tag{2.7}$$

The lateral-growth term can be expanded for $\frac{\partial R}{\partial \theta} \ll 1$ as

$$\frac{v}{R}[R^2 + (\frac{\partial R}{\partial \theta})^2]^{\frac{1}{2}} = \frac{v}{R}[R + \frac{1}{2R}(\frac{\partial R}{\partial \theta})^2 + ...] \approx v + \frac{v}{2R^2}(\frac{\partial R}{\partial \theta})^2. \tag{2.8}$$

The surface tension is taken to be proportional to the local curvature. At points on the surface with high curvature, the growth rate will be decreased; at points with low curvature, the growth rate will be increased. This will have the effect of relaxing the surface. For a ballistic deposition model, this would account for particles falling to a lower energy state, removing material from the sharp peaks to fill in the deep valleys. For a cell growth model, this would reflect a preference for new cells to be grown closer to the center of mass. The formula for curvature in polar coordinates is a standard result from differential geometry. The surface tension term can be expanded as

$$-\nu\frac{R^2 + 2(\frac{\partial R}{\partial \theta})^2 - R\frac{\partial^2 R}{\partial \theta^2}}{[R^2 + (\frac{\partial R}{\partial \theta})^2]^{\frac{3}{2}}} \approx \frac{-\nu R^2 - 2\nu(\frac{\partial R}{\partial \theta})^2 + \nu R\frac{\partial^2 R}{\partial \theta^2}}{R^3 + \frac{3}{2}R(\frac{\partial R}{\partial \theta})^2} \approx -\frac{\nu}{R} - \frac{2\nu}{R^3}(\frac{\partial R}{\partial \theta})^2 + \frac{\nu}{R^2}\frac{\partial^2 R}{\partial \theta^2}, \tag{2.9}$$

where we used $\frac{\partial R}{\partial \theta} \ll 1$, so that $R^3$ will dominate in the denominator.

We have a new radial stochastic differential equation, based on the BHW equation, but reduced using the small-gradient approximation:

$$\frac{\partial R(\Theta, t)}{\partial t} = v - \nu[\frac{1}{R} - \frac{1}{R^2}\frac{\partial^2 R}{\partial \theta^2} + \frac{2}{R^3}(\frac{\partial R}{\partial \theta})^2] + \frac{v}{R^2}(\frac{\partial R}{\partial \theta})^2 + \eta(\theta, t). \tag{2.10}$$

### 2.1.2 Properties of the Reduced BHW Equation

Recall that the original KPZ equation for $d = 1$ is

$$\frac{\partial h(\mathbf{x},t)}{\partial t} = \nu\frac{\partial^2 h}{\partial x} + \frac{\lambda}{2}(\frac{\partial h}{\partial x})^2 + \eta(\mathbf{x},t), \tag{2.11}$$

and compare with the reduced BHW equation (2.10). The effect of the using the radial curvature is two additional components of the surface-tension term: one proportional to $\frac{1}{R}$, the curvature of a circle, and another non-linear $(\frac{\partial R}{\partial \theta})^2$ term.

Several important properties of the BHW can be seen by inspection. First, there is a singularity at $R = 0$, so the equation does not describe the very initial stages of growth when the seed is part of the surface. Second, the equation is not invariant under translation in the radial direction, because of the explicit dependence on $R$. This is in contrast to the KPZ, which is invariant under translation in the growth direction. Hence the growth dynamics will necessarily change as the cluster grows and the surface propagates. This makes sense, since the quantities used in the geometric construction depends necessarily on the radius $R$. For small $R$, the local curvature will be greater because of the intrinsic curvature of the surface of small clusters; for large $R$, this intrinsic curvature of the surface should vanish.

It is natural to expect that a radial version of the KPZ equation would revert to the KPZ equation for a flat substrate in the large $R$ limit, since the surface of a spherical cluster grown from a single seed should lose its intrinsic curvature.

The BHW equation does indeed reduce to the KPZ equation in the limit $R \to \infty$. First recall that the KPZ equation has been already moved to the co-moving frame, so that the position function $h(x,t)$ gives the height above the mean height, whereas

the position function $R(\theta, t)$ in the BHW equation gives the radial height from the seed at the origin.

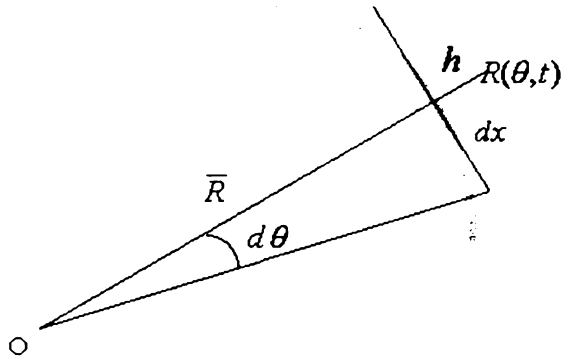


Figure 2.2: The relationship between the position function $R(\theta, t)$ in the radial geometry for growth from a seed at the origin, and the height function $h(x, t)$ of the KPZ equation. The surface interface is shown as the thick grey line.

Define $\bar{R} = vt$ to be the mean radius of the surface interface, propagating with mean velocity $v$. Then $dx = \bar{R}d\theta$, and $R = h + vt$. See Figure 2.2. Notice that $\frac{\partial R}{\partial \theta} = \bar{R}\frac{\partial h}{\partial x}$. Substituting into the reduced BHW equation, we have

$$\frac{\partial h}{\partial t} + v = v - \nu[\frac{1}{R} - \frac{\bar{R}^2}{R^2}\frac{\partial^2 h}{\partial x^2} + \frac{2\bar{R}^2}{R^3}(\frac{\partial h}{\partial x})^2] + \frac{\lambda \bar{R}^2}{2R^2}(\frac{\partial h}{\partial x})^2 + \eta \qquad (2.12)$$

Now as $R \to \infty$, we have only the following terms:

$$\frac{\partial h}{\partial t} = \nu\frac{\bar{R}^2}{R^2}\frac{\partial^2 h}{\partial x^2} + \frac{\lambda \bar{R}^2}{2R^2}(\frac{\partial h}{\partial x})^2 + \eta. \qquad (2.13)$$

Finally, as $R \to \infty$, we have $\frac{\bar{R}}{R} \to 1$ and we recover the KPZ equation, at least the deterministic part. The stochastic part of the equations will be investigated in the next subsection.

A radial continuum equation that describes radial Eden growth ought to obey Family-Vicsek scaling, which is confirmed by the discrete model presented later in this paper. To check the scale invariance of the reduced BHW equation, start with the equation in terms of $h$, already transformed to the co-moving frame, with the substitutions $\bar{R} = vt$, and $R = h + vt$.

$$\frac{\partial h}{\partial t} = -\nu[\frac{1}{h+vt} - \frac{(vt)^2}{(h+vt)^2}\frac{\partial^2 h}{\partial x^2} + \frac{2(vt)^2}{(h+vt)^3}(\frac{\partial h}{\partial x})^2] + \frac{\lambda(vt)^2}{2(h+vt)^2}(\frac{\partial h}{\partial x})^2 + \eta. \quad (2.14)$$

If $h(x,t)$ is self-affine, it should obey

$$h(x,t) = b^{-\alpha}h(bx, b^z t), \quad (2.15)$$

and so make the substitutions

$$h \to b^\alpha h, \qquad x \to bx, \qquad t \to b^z t, \quad (2.16)$$

resulting in

$$\begin{aligned}\frac{\partial h}{\partial t} &= -\nu[\frac{b^{z-\alpha}}{b^\alpha h + b^z vt} - \frac{(b^z vt)^2 b^{z-2}}{(b^\alpha h + b^z vt)^2}\frac{\partial^2 h}{\partial x^2} + \frac{2(b^z vt)^2 b^{\alpha+z-2}}{(b^\alpha h + b^z vt)^3}(\frac{\partial h}{\partial x})^2] \\ &\quad + \frac{\lambda(b^z vt)^2 b^{\alpha+z-2}}{2(b^\alpha h + b^z vt)^2}(\frac{\partial h}{\partial x})^2 + \eta. \end{aligned} \quad (2.17)$$

Now, using standard scaling arguments, assume that $\alpha < 1 < z$, expect the righthand side to be independent of $b$ in the hydrodynamic limit of $b \to \infty$. We see that the first and third component of the surface tension should vanish, and the ratio $\frac{(b^z vt)^2}{(b^\alpha h + b^z vt)^2}$ should tend to unity. Hence the $\frac{\partial^2 h}{\partial x^2}$ term should have the coefficient $b^{z-2}$, and the non-linear term $(\frac{\partial h}{\partial x})^2$ should have the coefficient $b^{\alpha+z-2}$. These are the same coefficients one gets when performing the same analysis on the original KPZ equation. Following Barabási and Stanley [3], who used the total derivative of the

Burgers equation to argue that the coefficient of the non-linear term should be zero, we recover the scaling relation $\alpha + z = 2$ for the radial case as well.

### 2.1.3 Random Noise in the Radial Geometry

Recall that the noise term in the KPZ equation is assumed to follow a Gaussian distribution with second moment following

$$\langle \eta(\mathbf{x}, t)\eta(\mathbf{x}', t')\rangle = 2D\delta^d(\mathbf{x} - \mathbf{x}')\delta(t - t'). \tag{2.18}$$

To investigate the noise term in the radial geometry, make the substitution $\theta = \frac{x}{\bar{R}}$, and use the property $\delta(ax) = a^{-1}\delta(x)$.

$$\langle \eta(\frac{x}{\bar{R}}, t)\eta(\frac{x'}{\bar{R}}, t')\rangle = 2D\delta(\frac{x}{\bar{R}} - \frac{x'}{\bar{R}})\delta(t - t'). \tag{2.19}$$

Noting that for any time $t$, $\bar{R}$ is constant as $x$ varies,

$$\langle \eta(\frac{x}{\bar{R}}, t)\eta(\frac{x'}{\bar{R}}, t')\rangle = \bar{R}2D\delta(x - x')\delta(t - t'), \tag{2.20}$$

$$\langle \bar{R}^{-1}\eta(\frac{x}{\bar{R}}, t)\eta(\frac{x'}{\bar{R}}, t')\rangle = 2D\delta(x - x')\delta(t - t'), \tag{2.21}$$

and hence in order to recover the Gaussian distribution, the left-hand side of the above equation must equal the left-hand side of Equation (2.18). Hence

$$\bar{R}^{-1}\eta(\frac{x}{\bar{R}}, t)\eta(\frac{x'}{\bar{R}}, t') = \eta(x, t)\eta(x', t'), \tag{2.22}$$

Notice that this will be satisfied if

$$\bar{R}^{-\frac{1}{2}}\eta(\frac{x}{\bar{R}}, t) = \eta(x, t), \tag{2.23}$$

Thus, the noise term in the BHW equation should be modified to a multiplicative noise $R^{-\frac{1}{2}}\eta(\theta, t)$, in order to recover the KPZ equation in the $R \to \infty$ limit.

## 2.2 Numerical Investigation of the 2D Radial Equation

In Batchelor, Henry and Watt's original numerical study on their equation in one dimension, they recovered $\beta \approx \frac{1}{3}$, but only for large times. However, from the scaling theory, the growth exponent $\beta$ is for early times, before saturation. Batchelor, Henry and Watt observed decreasing slopes which eventually appeared to approach a slope of $\frac{1}{3}$ in the log-log plot for $\beta$, but did not continue the simulation for larger times to see if the slope of $\frac{1}{3}$ persisted or continued to decrease. The decreasing slopes for early times could be due to the explicit dependence of their equation on $R$. The scaling behavior of the BHW equation should be contrasted with discrete model simulations in the radial geometry, including the off-lattice two-dimensional Eden model by C. Y. Wang, et.al. [43], and the 3D model presented later in this paper. In these cases, decreasing slopes are not observed, and the slope appears constant even over the early stages for growth. Hence, the BHW equation may not represent radial Eden growth.

To investigate further, a simple Euler finite-difference method is applied to both the original BHW Equation (2.1) and the reduced Equation (2.10), with similar results. The following discretization were used:

$$R(\theta, t) = R(i\Delta\theta, j\Delta t) = R_{i,j} \tag{2.24}$$

$$\text{noise}(\theta, t) = \text{noise}(i\Delta\theta, j\Delta t) = \text{noise}_{i,j} \tag{2.25}$$

$$\frac{\partial R}{\partial t} = \frac{R_{i,j+1} - R_{i,j}}{\Delta t} \tag{2.26}$$

$$R_\theta = \frac{R_{i+1,j} - R_{i-1,j}}{2\Delta\theta} \tag{2.27}$$

$$R_{\theta\theta} = \frac{R_{i+1,j} - 2R_{i,j} + R_{i-1,j}}{\Delta\theta^2} \tag{2.28}$$

Typically, $\Delta\theta = 2\pi/100$, and $\Delta t = 1/1000$ were used. Increasing the fineness of the mesh did not alter the results. The noise used took the form of bounded noise, with $+1$ and $-1$ chosen with equal probability. Changing the amplitude of the noise from 1 to 0.1 did not affect the results. Surfaces were typically grown from an initial condition of a circle of radius 2. The number of iterations used varied between $N = 100$ and $N = 1000$. Each iteration consisted of one time step (for example $1000\Delta t = 1$), so that $t = N$.

Periodically during the growth of the surface, the surface width $\sigma$ was computed, and logarithmic plots of $\sigma$ against $N$ (time) were generated and the slope $\beta$ was estimated. See Figure 2.3 for views of a typical surface.

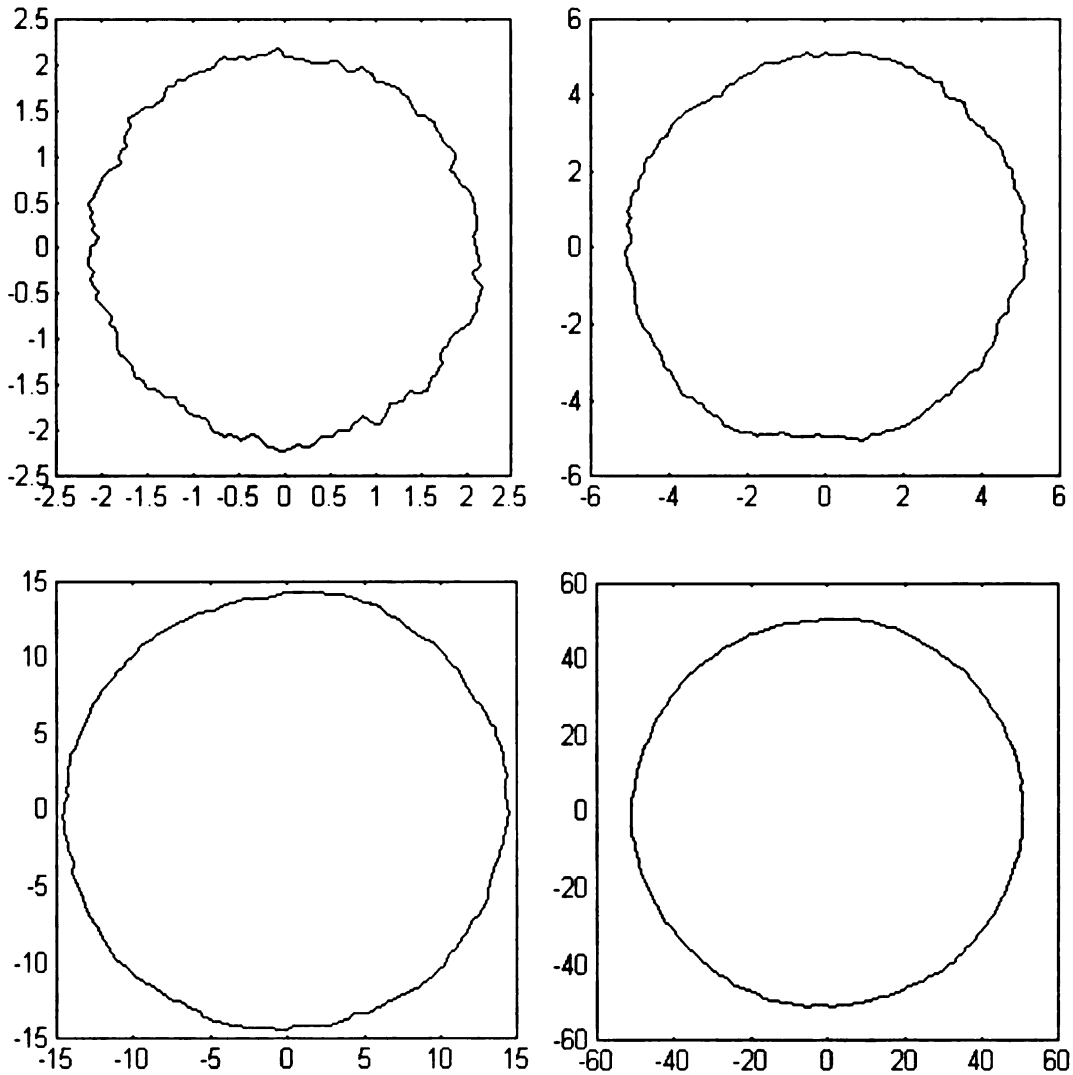


Figure 2.3: Snapshots of the growth of a surface grown from the 2D radial equation.

Integrating with the non-multiplicative, bounded noise, the results of Batchelor, Henry and Watt were not replicated. The slopes were too high (above 0.60), and tended to increase with time. However, taking the noise term to be $\eta(\theta, t) = \pm R^{-1/2}$, as suggested by the results of Section 2.1.3 above, resulted in slopes consistently near $\beta = 1/3$, as predicted by the scaling theory for the KPZ equation. See Figures 2.4 and 2.5 for two examples.

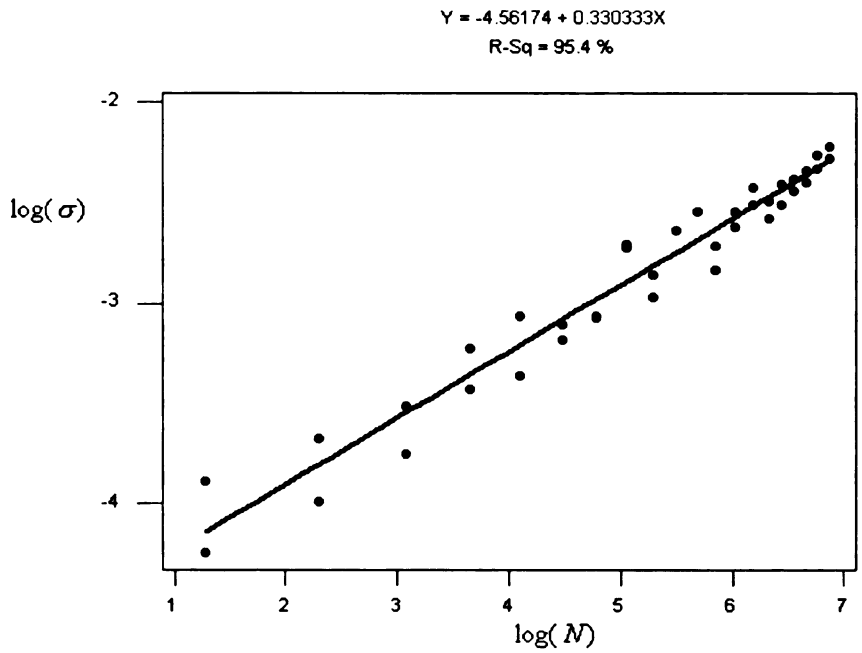


Figure 2.4: Regression plot for surface grown from the BHW equation with $v = 0.1$, $\nu = 0.1$, and noise $= \pm R^{-1/2}$.

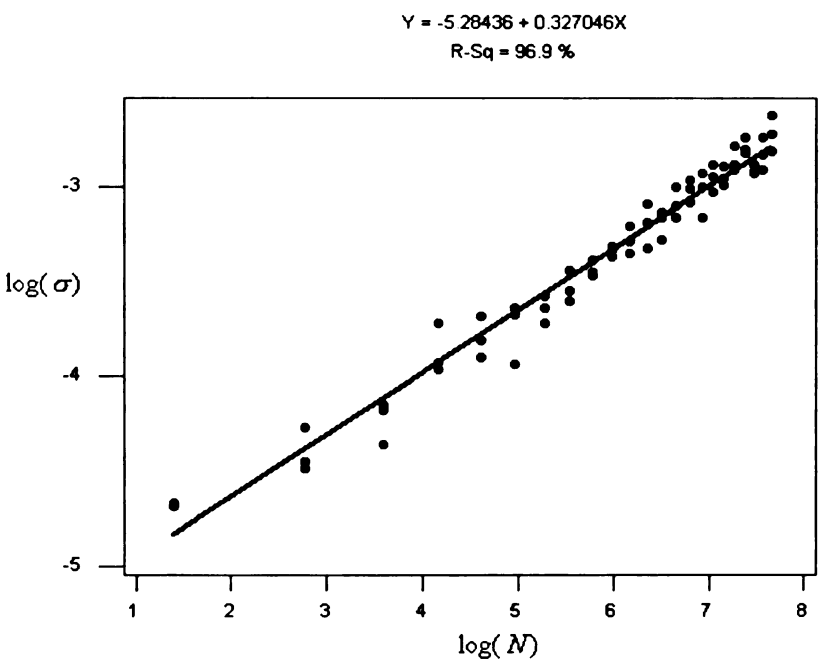


Figure 2.5: Regression plot for surface grown from the BHW equation with $v = 0.05$, $\nu = 0.005$, and noise $= \pm R^{-1/2}$.

Thus the numerical integration indicates that the two-dimensional radial growth equation

$$\frac{\partial R(\Theta,t)}{\partial t} = v - \nu[\frac{1}{R} - \frac{1}{R^2}\frac{\partial^2 R}{\partial \theta^2} + \frac{2}{R^3}(\frac{\partial R}{\partial \theta})^2] + \frac{v}{R^2}(\frac{\partial R}{\partial \theta})^2 + R^{\frac{-1}{2}}\eta(\theta,t) \qquad (2.29)$$

belongs to the KPZ universality class. It is interesting that while in the previous sections it was shown that the radial equation is equivalent to the KPZ equation in the large-radius limit, we have KPZ scaling properties persisting in the radial equation at early times. This is an indication of the stability of the KPZ scaling in the case $d = 1$.

## 2.3 Continuum Equation for Radial Surface Growth in 3D

A new continuum equation will now be introduced to model the growth of surfaces in three dimensions, such as 3D Eden cluster surfaces, using the radial geometry. The surface will be described by a function $R(\theta, \phi, t)$, where $R$ is the distance from the seed to the point at the spherical polar coordinates $(\theta, \phi)$ at time $t$. Following the KPZ equation and the BHW equation, three terms will be included: surface tension, lateral growth, and random noise.

### 2.3.1 Surface Tension

The surface tension will be taken to be negatively proportional to the mean curvature of the surface. The following is a standard result from differential geometry.

**Theorem 1** *Let $\boldsymbol{x} : \mathcal{U} \to \mathbb{R}^3$ be a regular patch of a surface. Then the mean curvature of the surface is given by the formula*

$$H = \frac{eG - 2fF + gE}{2(EG - F^2)}, \tag{2.30}$$

*where $E$, $F$, and $G$ are the coefficients of the first fundamental form, and $e$,$f$, and $g$ are the coefficients of the second fundamental form relative to $\boldsymbol{x}$.*

**Theorem 2** *If a surface in $\mathbb{R}^3$ is given by $R(\theta, \phi)$, then the mean curvature $H$ is given by*

$$\begin{aligned} H &= [2R^5 \sin^3\phi - R^4 R_\phi \cos\phi \sin^2\phi - 2R^2 R_\theta^2 R_\phi \cos\phi - R^2 R_\phi^3 \cos\phi \sin^2\phi \\ &\quad + 3R^3 R_\theta^2 \sin\phi + 3R^3 R_\phi^2 \sin^3\phi - R^4 R_{\theta\theta} \sin\phi - R^4 R_{\phi\phi} \sin^3\phi \\ &\quad - R^2 R_\phi^2 R_{\theta\theta} \sin\phi + 2R^2 R_\theta R_\phi R_{\theta\phi} \sin\phi - R^2 R_\theta^2 R_{\phi\phi} \sin\phi] \\ &\quad \Big/ [2R^3 (\sin^2\phi (R^2 + R_\phi^2) + R_\theta^2)^{\frac{3}{2}}]. \end{aligned} \tag{2.31}$$

**Proof** Let $\mathcal{U}$ be an open subset of $\mathbb{R}^2$ parameterized with coordinates $(\theta, \phi)$, and let $\mathbf{x} : \mathcal{U} \to \mathbb{R}^3$ be a patch, given by

$$\mathbf{x} = (R(\theta,\phi)\sin\phi\cos\theta, R(\theta,\phi)\sin\phi\sin\theta, R(\theta,\phi)\cos\phi). \tag{2.32}$$

.

The first-order derivatives of the patch are given by

$$\begin{aligned} \mathbf{x}_\theta &= (R_\theta \cos\theta \sin\phi - R\sin\theta\sin\phi, R_\theta \sin\theta \sin\phi + R\cos\theta\sin\phi, R_\theta \cos\phi), \\ \mathbf{x}_\phi &= (R_\phi \cos\theta \sin\phi + R\cos\theta\cos\phi, R_\phi \sin\theta \sin\phi + R\sin\theta\cos\phi, R_\phi \cos\phi - R\sin\phi). \end{aligned} \tag{2.33}$$

This is a regular patch, since

$$\begin{aligned}\mathbf{x}_\theta \times \mathbf{x}_\phi &= \Big((R\cos\theta\cos\phi + R_\phi\cos\theta\sin\phi)(-R\sin\theta\sin\phi + R_\theta\cos\theta\sin\phi),\\ &\quad (R\sin\theta\cos\phi + R_\phi\sin\theta\sin\phi)(R\cos\theta\sin\phi + R_\theta\sin\theta\sin\phi),\\ &\quad \cos\phi(R_\theta R_\phi\cos\phi - R\sin\phi)\Big) \qquad (2.34)\end{aligned}$$

is non-zero, assuming $R_\theta$ and $R_\phi$ both do not vanish at $\phi = 0$.

The second-order derivatives of the patch are given by

$$\begin{aligned}\mathbf{x}_{\theta\theta} &= \Big(\sin\phi(R_{\theta\theta}\cos\theta - 2R_\theta\sin\theta - R\cos\theta),\\ &\quad \sin\phi(R_{\theta\theta}\sin\theta + 2R_\theta\cos\theta - R\sin\theta), R_{\theta\theta}\cos\phi\Big), \qquad (2.35)\\ \mathbf{x}_{\theta\phi} &= \Big(R_{\theta\phi}\cos\theta\sin\phi + R_\theta\cos\theta\cos\phi - R_\phi\sin\theta\sin\phi - R\sin\theta\cos\phi, R_{\theta\phi}\sin\theta\sin\phi\\ &\quad + R_\theta\sin\theta\cos\phi + R_\phi\cos\theta\sin\phi + R\cos\theta\cos\phi, R_{\theta\phi}\cos\phi - R_\theta\sin\phi\Big), \qquad (2.36)\\ \mathbf{x}_{\phi\phi} &= \Big(\cos\theta(R_{\phi\phi}\sin\phi - 2R_\phi\cos\phi - R\sin\phi), \sin\theta(R_{\phi\phi}\sin\phi + 2R_\phi\cos\phi - R\sin\phi),\\ &\quad R_{\phi\phi}\cos\phi - 2R_\phi\sin\phi - R\cos\phi\Big). \qquad (2.37)\end{aligned}$$

From these derivatives, we may compute the coefficients of the first and second fundamental forms; that is:

$$E = \mathbf{x}_\theta \cdot \mathbf{x}_\theta, \quad F = \mathbf{x}_\theta \cdot \mathbf{x}_\phi, \quad G = \mathbf{x}_\phi \cdot \mathbf{x}_\phi, \qquad (2.38)$$

and

$$e = \frac{\mathbf{x}_{\theta\theta}\cdot(\mathbf{x}_\theta \times \mathbf{x}_\phi)}{\sqrt{EG - F^2}}, \quad f = \frac{\mathbf{x}_{\theta\phi}\cdot(\mathbf{x}_\theta \times \mathbf{x}_\phi)}{\sqrt{EG - F^2}}, \quad g = \frac{\mathbf{x}_{\phi\phi}\cdot(\mathbf{x}_\theta \times \mathbf{x}_\phi)}{\sqrt{EG - F^2}}. \qquad (2.39)$$

Then, by substituting into the formula for mean curvature (Equation (2.30)) and much simplification, we have the mean curvature of a surface given by $R(\theta, \phi)$.

□

Next it will be investigated whether the mean curvature in the radial geometry reduces to the $\nabla^2 h$ term of the Edwards-Wilkinson equation and the KPZ equation. Proceeding as in the $d = 1$ case, write $h = R - \bar{R}$, where $\bar{R} = vt$ and $v$ is the mean growth velocity. Transforming coordinates, we have

$$dx = \bar{R}\sin\phi d\theta, \quad dy = \bar{R}d\phi, \tag{2.40}$$

and so

$$R_\theta = \bar{R}\sin\phi h_x, \quad R_\phi = \bar{R}h_y. \tag{2.41}$$

Substituting into the expression for the mean curvature in the proposition (Equation (2.31)), we have

$$\begin{aligned} H &= [2R^5\sin^3\phi - R^4\bar{R}h_y\cos\phi\sin^2\phi - 2R^2\bar{R}^3h_x^2h_y\cos\phi\sin^2\phi - R^2\bar{R}^3h_y^3\cos\phi\sin^2\phi \\ &\quad +3R^3\bar{R}^2h_x^2\sin^3\phi + 3R^3\bar{R}^2h_y^2\sin^3\phi - R^4\bar{R}^2h_{xx}\sin^3\phi - R^4\bar{R}^2h_{yy}\sin^3\phi \\ &\quad -R^2\bar{R}^4h_y^2h_{xx}\sin^3\phi + 2R^2\bar{R}^4h_xh_yh_{xy}\sin^3\phi - R^2\bar{R}^4h_x^2h_{yy}\sin^3\phi] \\ &\quad \Big/[2R^3(\sin^2\phi(R^2+\bar{R}^2h_y^2) + \bar{R}^2h_x^2\sin^2\phi)^{\frac{3}{2}}] \end{aligned} \tag{2.42}$$

Write the denominator as $2R^6\sin^3\phi(1+\frac{\bar{R}^2}{R^2}h_x^2+\frac{\bar{R}^2}{R^2}h_y^2)^{\frac{3}{2}}$, and then canceling a common factor of $2R^6\sin^3\phi$, we have

$$\begin{aligned} H &= [\frac{2}{R} - \frac{\bar{R}}{R^2}h_y\cot\phi - 2\frac{\bar{R}^3}{R^4}h_x^2h_y\cot\phi - \frac{\bar{R}^3}{R^4}h_y^3\cot\phi \\ &\quad +3\frac{\bar{R}^2}{R^3}h_x^2 + 3\frac{\bar{R}^2}{R^3}h_y^2 - \frac{\bar{R}^2}{R^2}h_{xx} - \frac{\bar{R}^2}{R^2}h_{yy} \\ &\quad -\frac{\bar{R}^4}{R^4}h_y^2h_{xx} + 2\frac{\bar{R}^4}{R^4}h_xh_yh_{xy} - \frac{\bar{R}^4}{R^4}h_x^2h_{yy}] \\ &\quad \Big/[2(1+\frac{\bar{R}^2}{R^2}h_x^2+\frac{\bar{R}^2}{R^2}h_y^2)^{\frac{3}{2}}] \end{aligned} \tag{2.43}$$

Now, in the limit $R \to \infty$, we have $\frac{\bar{R}}{R} \to 1$, and so

$$H \approx \frac{-h_{xx} - h_{yy} - h_y^2 h_{xx} + 2h_x h_y h_{xy} - h_x^2 h_{yy}}{2(1 + h_x^2 + h_y^2)^{\frac{3}{2}}} \tag{2.44}$$

In the small-gradient approximation, we have $H \approx \frac{1}{2}(h_{xx} + h_{yy}) = \frac{1}{2}\nabla^2 h$, which is the surface-tension term used in the KPZ equation.

Returning to the mean curvature in the radial geometry, Equation (2.31), we see that in the small-gradient approximation, the denominator is dominated by $2\sin^3\phi R^6$. Following some cancellations, we have

$$\begin{aligned} H \approx\ & \frac{1}{R} - \frac{1}{2R^2} R_\phi \cot\phi - \frac{1}{R^4} R_\theta^2 R_\phi \cot\phi \csc^2\phi - \frac{1}{2R^4} R_\phi^3 \cot\phi \\ & + \frac{3}{2R^3}(R_\theta^2 \csc^2\phi + R_\phi^2) - \frac{1}{2R^2}(R_{\theta\theta}\csc^2\phi + R_{\phi\phi}) \\ & - \frac{1}{2R^4}\csc^2\phi(R_\phi^2 R_{\theta\theta} - 2R_\theta R_\phi R_{\theta\phi} + R_\theta^2 R_{\phi\phi}) \end{aligned} \tag{2.45}$$

### 2.3.2 Lateral Growth

For lateral growth in the radial geometry in three dimensions, proceed according to Figure 2.6, which is similar to Figure 2.1 for two dimensions. A point $R(\theta, \phi, t)$ is shown on the surface, represented in the figure by the tangent plane. The lateral growth we are interested in is in the direction normal to the tangent plane. Over a small time increment of $\delta t$, a surface propagating with average velocity $v$ will advance $v\delta t$ in the normal direction, and $\delta R$ in the radial direction. There will also be corresponding changes in the coordinates $\theta$ and $\phi$. Notice in Figure 2.6, the angle shown at the origin is generally not in either coordinate direction, but may be considered the result of a sequence of changes in the coordinate directions.

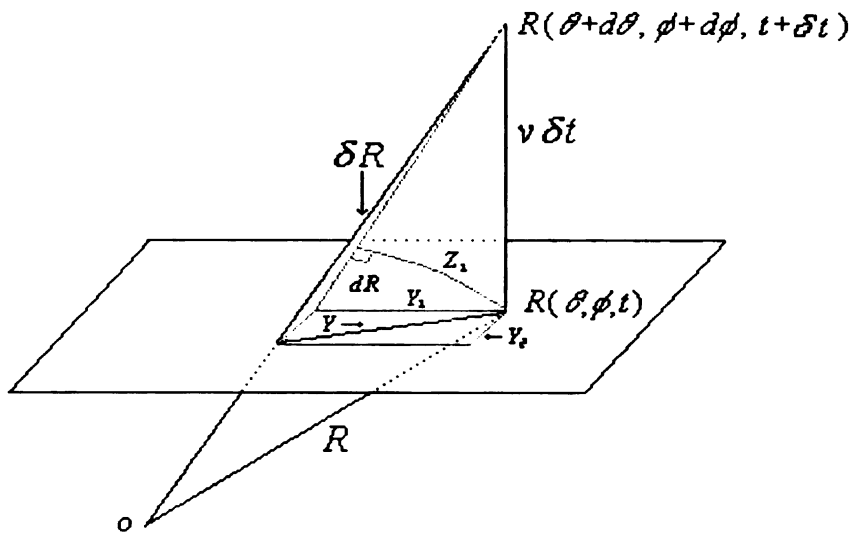


Figure 2.6: Lateral growth in the radial geometry in three dimensions. The tangent plane to the surface at the point $R(\theta, \phi, t)$ is shown.

I'll focus first on the $\phi$ coordinate. In Figure 2.6, the segments shown with lengths $dR$, $Z_1$, and $Y_1$ all lie in plane $\theta$ = constant. Holding $t$ fixed, a change in $\phi$ of $d\phi$ will result in a change of $dR$ away from the tangent plane, and sweep out the arc with length $Z_1$. We then have

$$Z_1 = R\sin(d\phi) \approx Rd\phi, \tag{2.46}$$

and by using similar triangles, we have

$$\frac{v\delta t}{Y_1} = \frac{Rd\phi}{dR}, \tag{2.47}$$

$$Y_1 = \frac{v\delta t}{R}\frac{dR}{d\phi}, \tag{2.48}$$

where $Y_1$ lies on the tangent plane and represents the $\phi$ component of the angular change.

Similarly, holding $t$ fixed, a change in $\theta$ of $d\theta$ will result in a change of $dR$ away from the tangent plane, and sweep out the arc with length $Z_2$. For clarity, these

quantities have been omitted from Figure 2.6. We then have

$$Z_2 = R\sin\phi\sin(d\theta) \approx R\sin\phi d\theta, \tag{2.49}$$

and by using similar triangles, we have

$$\frac{v\delta t}{Y_2} = \frac{R\sin\phi d\theta}{dR}, \tag{2.50}$$

$$Y_2 = \frac{v\delta t}{R\sin\phi}\frac{dR}{d\theta}, \tag{2.51}$$

where $Y_2$ lies on the tangent plane and represents the $\theta$ component of the angular change.

Now, by the Pythagorean Theorem, we have

$$Y^2 = Y_1^2 + Y_2^2 \tag{2.52}$$

$$Y^2 = (\frac{v\delta t}{R}\frac{dR}{d\theta})^2 + (\frac{v\delta t}{R\sin\phi}\frac{dR}{d\theta})^2 \tag{2.53}$$

$$Y^2 = (\frac{v\delta t}{R})^2[(\frac{dR}{d\phi})^2 + \frac{1}{\sin^2\phi}(\frac{dR}{d\theta})^2] \tag{2.54}$$

Finally, again by the Pythagorean Theorem (see Figure 2.6), we have

$$(\delta R)^2 = (v\delta t)^2 + (\frac{v\delta t}{R})^2[(\frac{dR}{d\phi})^2 + \frac{1}{\sin^2\phi}(\frac{dR}{d\theta})^2] \tag{2.55}$$

$$(\delta R)^2 = \frac{(v\delta t)^2}{R^2}[R^2 + (\frac{dR}{d\phi})^2 + \frac{1}{sin^2\phi}(\frac{dR}{d\theta})^2]. \tag{2.56}$$

Finally, by letting $\delta t \to 0$, we have the lateral growth term for the component of the growth velocity in the locally normal direction as

$$\frac{\partial R}{\partial t} = \frac{v}{R}[R^2 + R_\phi^2 + \csc^2\phi R_\theta^2]^{\frac{1}{2}}. \tag{2.57}$$

If one uses a small-gradient approximation $R_\phi^2 + \csc^2\phi R_\theta^2 \ll R^2$ the lateral growth term can be reduced to

$$v[1 + \frac{R_\phi^2 + \csc^2\phi R_\theta^2}{R^2}]^{\frac{1}{2}} \approx v + \frac{v}{2R^2}(R_\phi^2 + \csc^2\phi R_\theta^2) \tag{2.58}$$

Next it will be investigated whether the lateral growth term in the radial geometry reduces to the non-linear term of the KPZ equation. Proceeding as before, write $h = R - \bar{R}$ and so $R_\theta = \bar{R}\sin\phi h_x$, and $R_\phi = \bar{R}h_y$.

So the lateral growth term is transformed to

$$\frac{v}{R}[R^2 + \bar{R}^2 h_y^2 + \frac{1}{\sin^2\phi}\bar{R}^2\sin^2\phi h_x^2]^{\frac{1}{2}}, \tag{2.59}$$

or

$$v[1 + \frac{\bar{R}^2}{R^2}h_y^2 + \frac{\bar{R}^2}{R^2}h_x^2]^{\frac{1}{2}}. \tag{2.60}$$

So in the large radius limit, $R \to \infty$, and $\frac{\bar{R}^2}{R^2} \to 1$, and we have

$$v[1 + (\nabla h)^2]^{\frac{1}{2}}, \tag{2.61}$$

which is the lateral growth term in the flat substrate geometry used in the KPZ equation.

### 2.3.3 Random Noise and the Simplified 3D Radial Equation

Following the results of Section 2.1.3, the random noise in three dimensions will be assumed to be of the form

$$R^{-a}\eta(\theta, \phi, t), \tag{2.62}$$

where the stochastic function $\eta(\theta, \phi, t)$ satisfies a Gaussian distribution

$$\langle\eta(\Theta, t)\rangle = 0, \quad \text{and} \quad \langle\eta(\Theta, t)\eta(\Theta', t')\rangle = 2D\delta^2(\Theta - \Theta')\delta(t - t'), \tag{2.63}$$

and $\Theta = (\theta, \phi)$.

The proposed continuum equation for radial surface growth in three dimensions is thus

$$\frac{\partial R(\theta,\phi,t)}{\partial t} = -\nu H + \frac{v}{R}[R^2 + R_\phi^2 + \csc^2\phi R_\theta^2]^{\frac{1}{2}} + R^{-a}\eta(\theta,\phi,t), \tag{2.64}$$

where $H$ is the surface curvature given by Equation (2.31).

To preserve rotation and inversion symmetry with respect to the coordinates $\theta$ and $\phi$, we can rule out the inclusion of odd-order derivatives such as $R_\theta$, and $R_\phi^3$ in the surface curvature term. Note that the inclusion of important factors such as $R_\theta^2$ and $\csc^2\phi$ do not violate this symmetry.

Then the equation becomes

$$\begin{aligned}\frac{\partial R}{\partial t} &= -\nu[\frac{1}{R} + \frac{3}{2R^3}(R_\theta^2\csc^2\phi + R_\phi^2) - \frac{1}{2R^2}(R_{\theta\theta}\csc^2\phi + R_{\phi\phi}) \\ &\quad -\frac{1}{2R^4}\csc^2\phi(R_\phi^2 R_{\theta\theta} + R_\theta^2 R_{\phi\phi})] + \frac{v}{R}[R^2 + R_\phi^2 + \csc^2\phi R_\theta^2]^{\frac{1}{2}} + R^{-a}\eta(\theta,\phi,t).\end{aligned} \tag{2.65}$$

Assuming that the fourth-order derivatives are irrelevant to scaling compared to second-order derivatives [3], we can pare down the surface curvature term even further. Finally, using the small-gradient approximation to reduce the lateral growth term (see Equation (2.58)), we have a simple continuum equation for radial surface growth in three dimensions:

$$\begin{aligned}\frac{\partial R}{\partial t} &= -\nu[\frac{1}{R} + \frac{3}{2R^3}(R_\theta^2\csc^2\phi + R_\phi^2) - \frac{1}{2R^2}(R_{\theta\theta}\csc^2\phi + R_{\phi\phi})] \\ &\quad v + \frac{v}{2R^2}[R_\phi^2 + \csc^2\phi R_\theta^2] + R^{-a}\eta(\theta,\phi,t),\end{aligned}$$

or

$$\frac{\partial R}{\partial t} = v - \frac{\nu}{R} + \frac{vR - 3\nu}{2R^3}[R_\phi^2 + \csc^2\phi R_\theta^2] - \frac{\nu}{2R^2}[R_{\phi\phi} + \csc^2\phi R_{\theta\theta}] + R^{-a}\eta(\theta,\phi,t). \tag{2.66}$$

## 2.4 Numerical Investigation of the 3D Equation

A simple Euler finite-difference method was applied to Equation (2.66). Using the reduced Equation (2.66) instead does not perceptively change the results. The following discretizations were used:

$$R(\theta,\phi,t) = R(i\Delta\theta, j\Delta\phi, k\Delta t) = R_{i,j,k} \tag{2.67}$$

$$\text{noise}(\theta,\phi,t) = \text{noise}(i\Delta\theta, j\Delta\phi, k\Delta t) = \text{noise}_{i,j,k} \tag{2.68}$$

$$\frac{\partial R}{\partial t} = \frac{R_{i,j,k+1} - R_{i,j,k}}{\Delta t} \tag{2.69}$$

$$R_\theta = \frac{R_{i+1,j,k} - R_{i-1,j,k}}{2\Delta\theta} \tag{2.70}$$

$$R_\phi = \frac{R_{i,j+1,k} - R_{i,j-1,k}}{2\Delta\phi} \tag{2.71}$$

$$R_{\theta\theta} = \frac{R_{i+1,j,k} - 2R_{i,j,k} + R_{i-1,j,k}}{\Delta\theta^2} \tag{2.72}$$

$$R_{\phi\phi} = \frac{R_{i,j+1,k} - 2R_{i,j,k} + R_{i,j-1,k}}{\Delta\phi^2} \tag{2.73}$$

$$R_{\theta\phi} = \frac{R_{i+1,j+1,k} - R_{i+1,j-1,k} - R_{i-1,j+1,k} + R_{i-1,j-1,k}}{4\Delta\theta\Delta\phi} \tag{2.74}$$

For all of the results shown below, $\Delta\theta = 2\pi/100$, $\Delta\phi = 2\pi/50$, and $\Delta t = 1/1000$ were used. The noise used took the form of bounded noise, with $+1$ and $-1$ chosen with equal probability. Changing the amplitude of the noise from 1 to 0.1 did not affect the results. For many of the simulations this bounded noise was multiplied by some decreasing function of $R$. Surfaces were typically grown from an initial condition of a sphere of radius 2. The number of iterations used varied between $N = 400$ and $N = 900$. Each iteration consisted of one time step (for example $1000\Delta t = 1$), so that $t = N$.

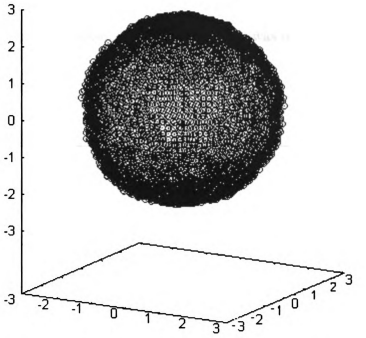


Figure 2.7: Surface grown with $v = .001$, $\nu = .001$, with $\eta = \pm R^{-1}$.

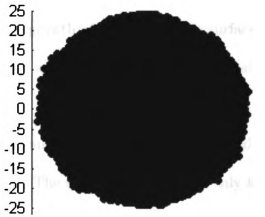


Figure 2.8: 2D projection of a typical surface grown with the 3D equation.

Depending on the specified velocity, this would grow surfaces out to a mean radius in the range of about 5 to about 50. See Figures 2.7 and 2.8 for examples of typical surfaces grown using the continuum equation. Also it was noted that the mean radius $\bar{R}$ varied linearly with time, see Figure 2.9.

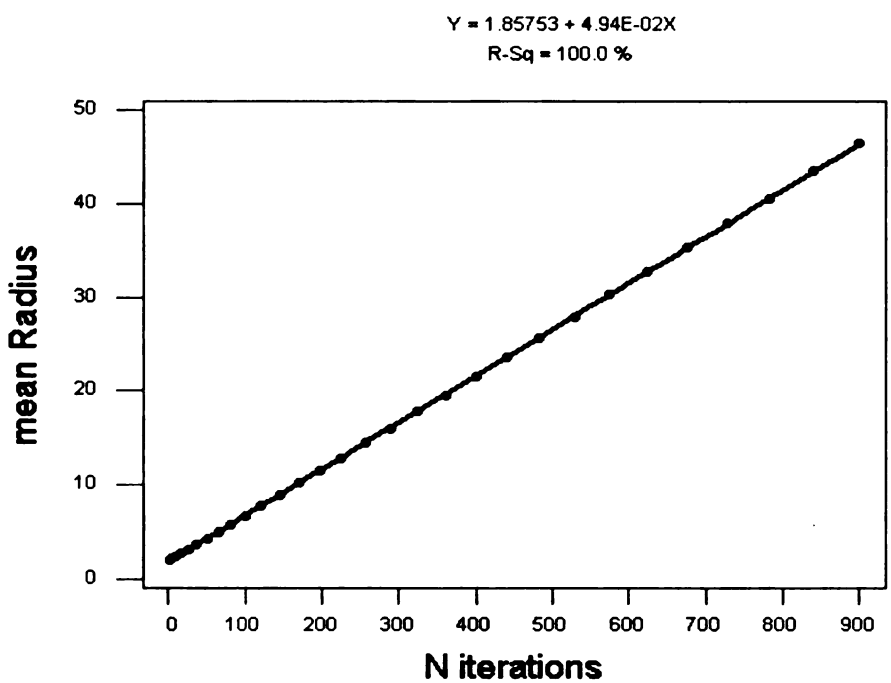


Figure 2.9: Plot of mean radius against number of iterations.

Periodically during the growth of the surface, the surface width $\sigma$ was computed, and logarithmic plots of $\sigma$ against $N$ (time), were generated and the slope $\beta$ was estimated.

First, growth without multiplicative noise was simulated. That is, the noise term was simply $\eta(\theta, \phi, t) = \pm 1$. The slope $\beta$ was constant only for very early times, then quickly increased so that the log plots of $\sigma$ against $N$ were concave up. See Figure 2.10 for a typical result. The slope for early times in the figure is approximately 0.22, and for late times, the slope increases to above 0.5.

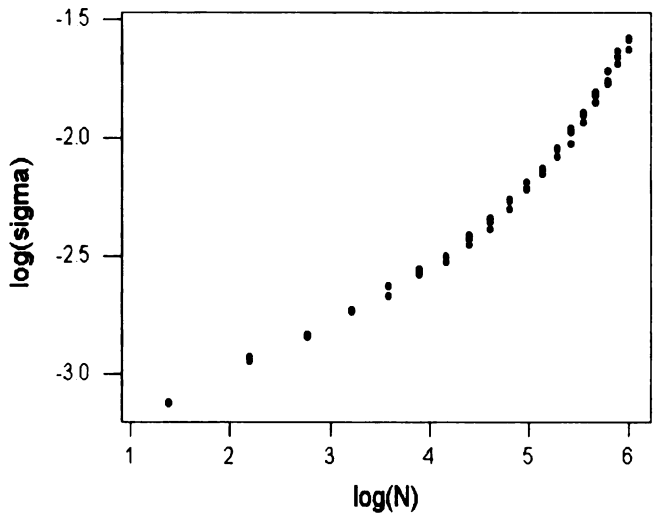


Figure 2.10: Regression for surface grown with $v = .01$, $\nu = .001$, and $\eta = \pm 1$.

The effect of modifying the noise term to take the form of a multiplicative noise $\pm R^{-a}$ for some $a > 0$ is to prolong the time period over which the slope $\beta$ remains constant. Using $a = 1/2$, as in the two-dimensional case, had surprisingly good results. Decreasing the noise slightly further to $a = 2/3$ resulted in the best linear plots, while taking $a = 1$ created plots that were concave down, as the noise became insignificant and the surface smoothed.

Depending on the choice of the parameters ($\nu$ for surface tension and $v$ for velocity, the plots consistently showed a crossover from a small-slope regime with $\beta \approx 0.12$ to a large-slope regime, with $\beta \approx 0.22$. These are significant values for the growth exponent $\beta$, since the small-slope value is consistent with the results from the discrete model discussed in the next chapter, and the large-slope value is consistent with several numerical investigations of the KPZ equation (please refer back to Table 1.1).

The small-slope regime is dominant when the surface tension $\nu$ is large compared to the velocity $v$, and the large-slope regime dominates when the surface tension is small compared to the velocity. The three figures below illustrate the crossover as $\nu$ increases for simulations with velocity $v = 0.01$ and noise $= \pm R^{-1/2}$.

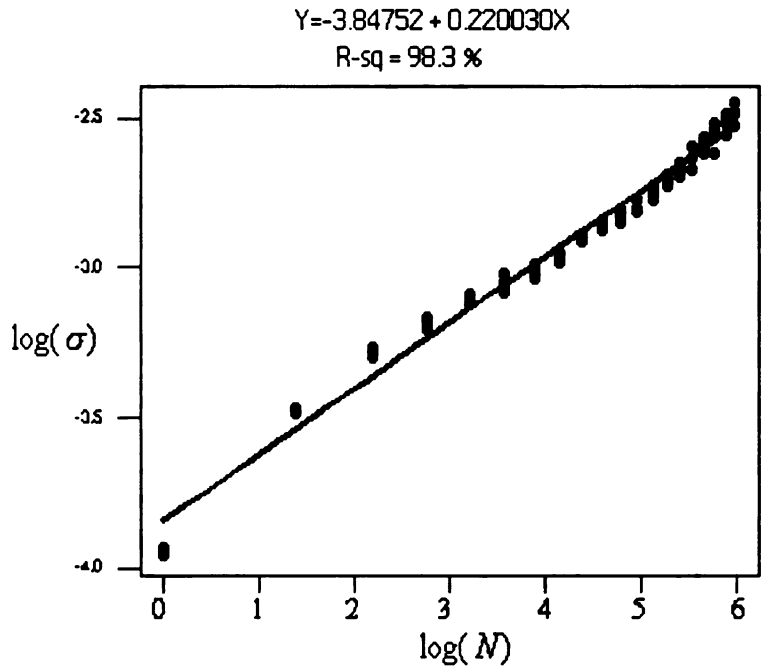


Figure 2.11: Regression plot for surface grown with $v = .01$, $\nu = .001$, and noise $= \pm R^{-1/2}$. This is the large $\beta$ regime.

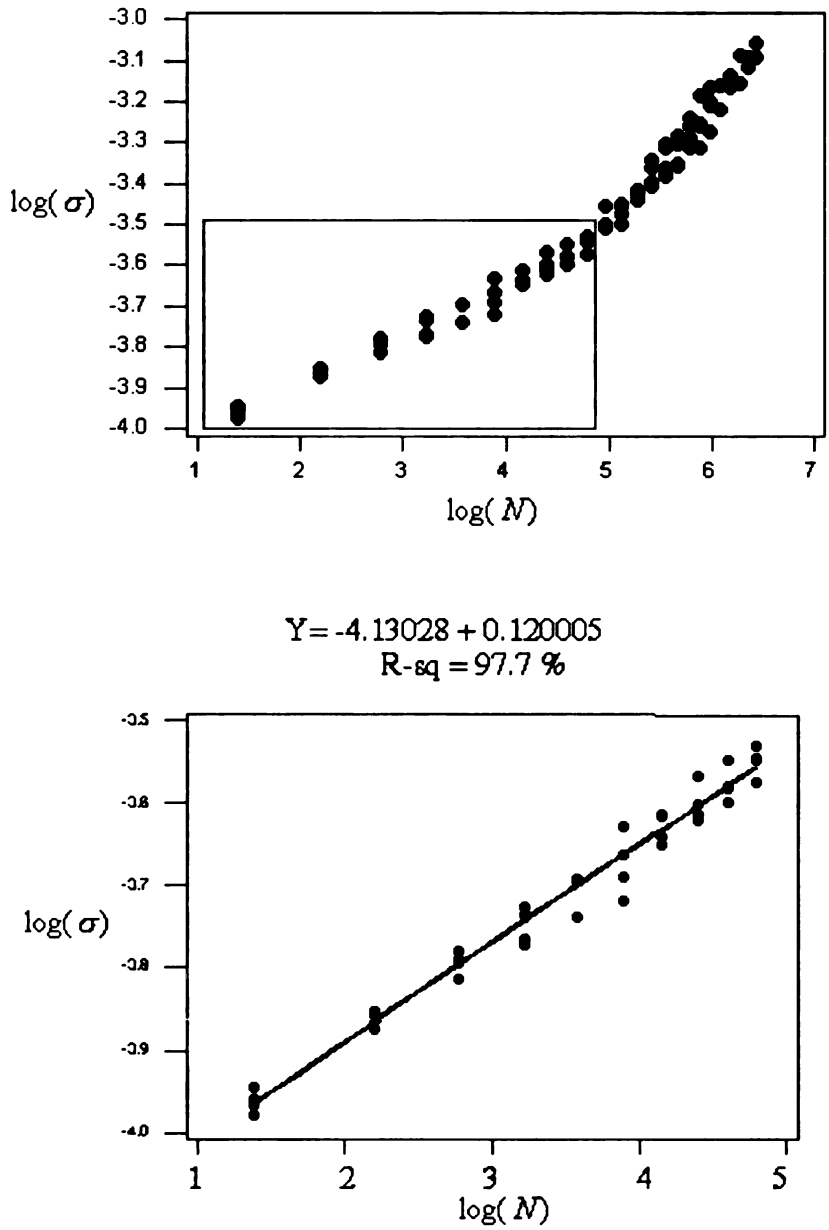


Figure 2.12: Regression plot for surface grown with $v = .01$, $\nu = .001$, and noise $= \pm R^{-1/2}$, showing a slope of $\beta \approx 0.12$ for early times, then crossing over to a large-slope regime. The highlighted portion of the upper plot is magnified and shown in the lower plot.

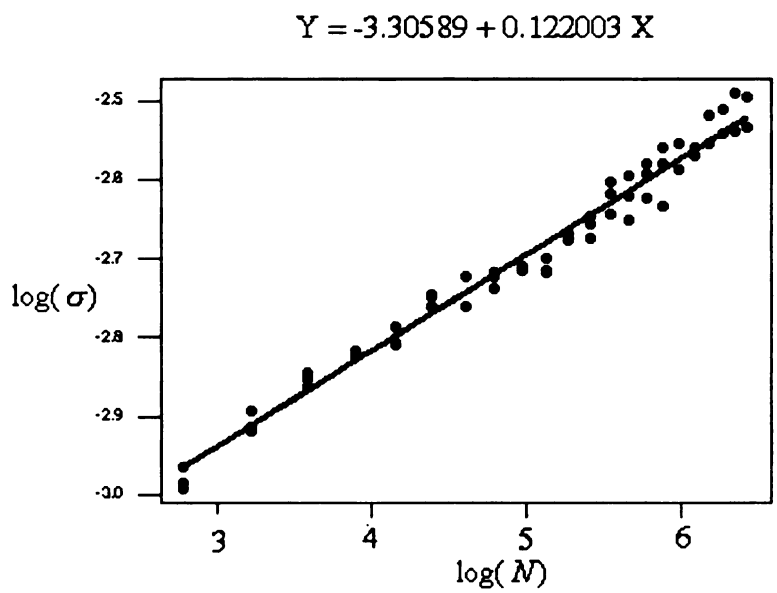


Figure 2.13: Regression plot for surface grown with $v = .001$, $\nu = .001$, and noise $= \pm R^{-1/2}$, showing a slope of $\beta \approx 0.12$, and no crossover to a large-slope regime. Here the velocity does not appear to dominate the surface tension.

Lastly, simulations with a noise term $\eta = \pm R^{-2/3}$ were conducted. This formulation of the noise appears to preserve a constant slope for longer time periods. Again, when the velocity dominates over surface tension, the value for the growth exponent $\beta$ is near 0.22, but as surface tension increases, the growth exponent crosses over to a small-slope regime near 0.12. With a high velocity, the surface grows more quickly and skips over the small-slope regime. See Figure 2.14. Only when the surface is grown slowly is there information for the surface when it is still relatively small, and then for these early times, the growth exponent $\beta$ is found to be near 0.12. See Figures 2.15 - 2.17.

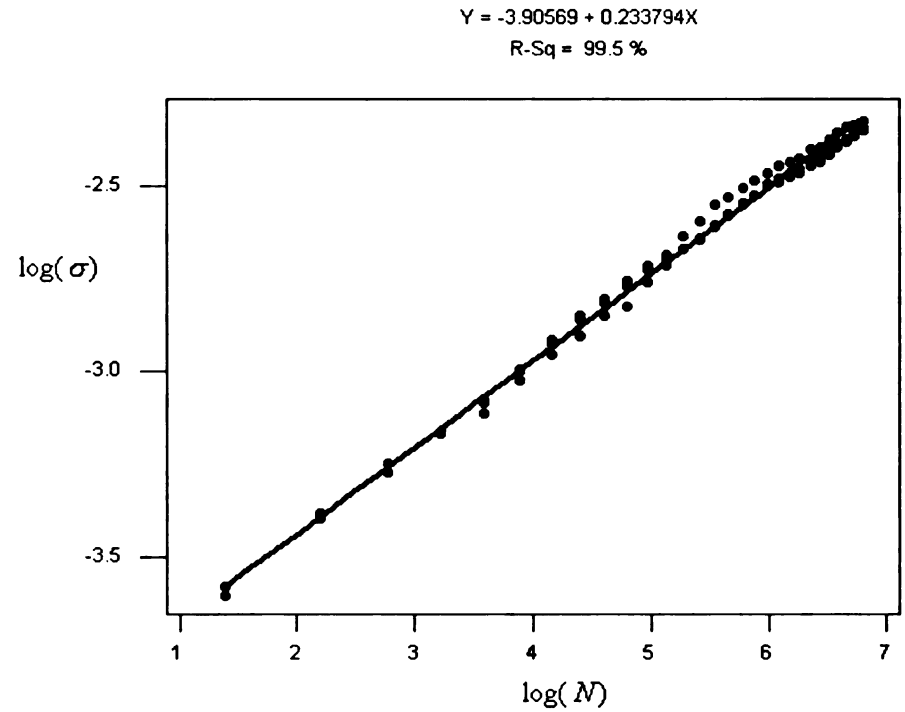


Figure 2.14: Regression plot for surface grown with $v = .05$, $\nu = .001$, and noise $= \pm R^{-2/3}$, showing a slope of $\beta \approx 0.23$. There is no crossover from a small-slope regime, since the velocity is relatively high.

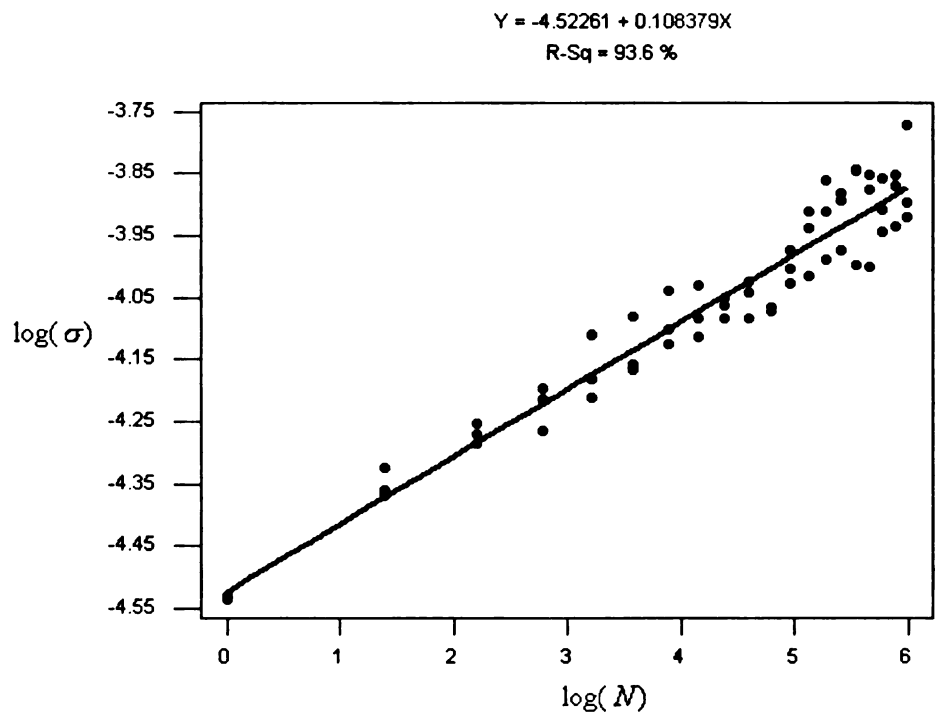


Figure 2.15: Regression plot for surface grown with $v = .01 = \nu$, and noise $= \pm R^{-2/3}$, showing a slope of $\beta \approx 0.11$, and no crossover yet to a large-slope regime.

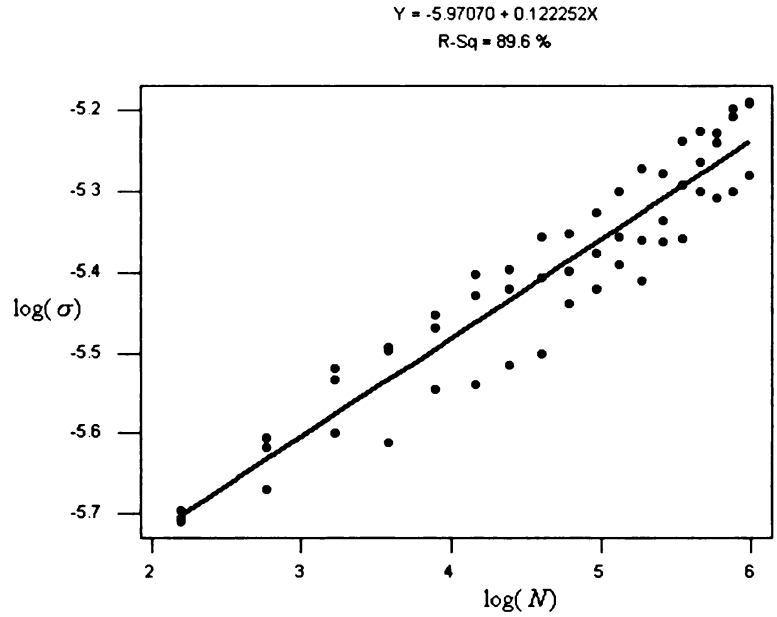


Figure 2.16: Regression plot for surface grown with $v = .005$, $\nu = .001$, and noise $= \pm R^{-2/3}$, showing a slope of $\beta \approx 0.13$, and no crossover yet to a large-slope regime.

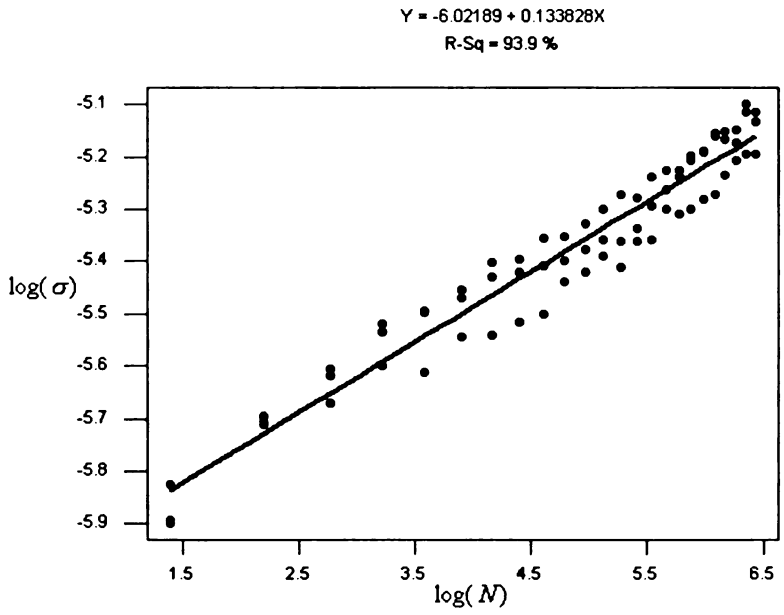


Figure 2.17: Regression plot for surface grown with $v = .005$, $\nu = .001$, and noise $= \pm 0.1 R^{-2/3}$. The noise amplitude is smaller, yet the results are similar to those in the previous figure.

In summary, numerical investigation of the three-dimensional radial growth equation exhibits two distinct scaling regimes. For early times, there is a small-$\beta$ regime, where $\beta$ is consistently found to be near 0.12. Then there is a crossover to a large-$\beta$ regime, where $\beta$ is consistently found to be near 0.22. The crossover appears to be strongly effected by the coupling of the velocity $v$ and the surface tension $\nu$. It is interesting that both small-$\beta$ and large-$\beta$ results have been found separately in previous numerical investigations of the KPZ equation. However most, including all of the recent studies, report a value consistent with the large-$\beta$ regime. A crossover between two scaling regimes for the growth exponent $\beta$ is not known to have been reported in any previous study of the KPZ equation.

It was shown in Chapter 2 that the radial equation reduces to the KPZ equation in the large-radius limit as expected. This is consistent with the numerical simulations, where it is observed that for large $R$, the scaling behavior crosses over to a regime where the growth exponent $\beta$ is similar to those reported in several recent numerical and analytical studies of the KPZ equation [7, 9, 31]. However, unlike the two-dimensional case explored in Section 2.2, this behavior does not persist for early times, indicating an instability in the coupling behavior of the radial growth equation.

It is conjectured that for early times in the radial geometry, where the intrinsic curvature of the surface is still significant, the surface tension dominates the coupling, and the scaling behavior starts out in the small-slope regime for the growth exponent. As the radius grows, however, the intrinsic curvature and thus the surface tension becomes less influential, and eventually a crossover threshold is reached and the scaling of the growth exponent enters the large-slope regime.

# Chapter 3

# A New Discrete Model for Three-dimensional Radial Surface Growth

The Eden model for cluster growth in two dimensions is understood to be in the KPZ universality class for $d = 1$, but the scaling behavior of this discrete model is not certain in three dimensions. Previous studies of the Eden model in three dimensions have all been implemented on a lattice, and mostly using the flat substrate geometry. As explained in Section 1.2, Eden clusters grown on a lattice exhibit significant anisotropies, which should not be present in the physical case.

In Section 2.4, a numerical investigation of the radial continuum equation for rough surface growth in three dimensions indicated two distinct scaling regimes, which has not been observed in any previous discrete model. It was conjectured that this behavior may be due to the use of the radial geometry. Thus, an investigation of an off-lattice Eden model using the radial geometry in three dimensions may prove to be beneficial.

In this chapter, a three-dimensional off-lattice Eden cluster growth model is introduced. One theoretical algorithm is discussed, and two numerical algorithms are implemented to grow eden clusters in large-scale simulations. Several properties of the model are discussed, including the density and the compactness of the clusters.

Lastly, the scaling properties of the surface width is investigated, and compared with the predictions of the KPZ equation and the radial equation discussed in Chapter 2.

## 3.1 Basics of the Off-lattice Three-dimensional Eden Model

Each cell of the cluster is represented as a node in space, with a minimal distance between nodes normalized to 1. The nodes are in fact the centers of the cells, which can be thought of as solid spherical balls of radius $\frac{1}{2}$. Starting with the seed node at the origin, the second node must be added at a distance 1 away (so that its cell is tangent to the seed cell). Since there is no underlying lattice, the second node can lie anywhere on a sphere radius 1 away from the seed node.

At each iteration step, to add another node, at first one of the existing "live" nodes of the cluster is chosen to receive new growth (see version C in Section 1.2), called a "test" node. Then a location for the new growth is chosen at random, at a distance 1 away from the test node, as before. However, since the new cell cannot overlap with any of the other existing cells of the cluster, the new location cannot be within a distance 1 from the any of the other nodes. If no site can be chosen, in which case there are too many nearby cells blocking new growth, the test node is declared "dead", and will not be selected again for new growth. Please refer back to Figure 1.1 for a typical off-lattice Eden cluster.

## 3.2 Selecting a Location for New Growth

Once a existing live cell has been selected for new growth, the question is how to determine a location for new growth which is unblocked on the unit sphere. Outlined below are three different methods.

### 3.2.1 Theoretical Sure-fire Method

Let $c$ be the current live cell chosen at random to receive new growth at the point $t$. Let $S$ denote the unit sphere with center $c$, which contains the set of all possible locations for growth. Ideally, we would want to check which areas on $S$ are blocked for growth be neighboring cells. Suppose point $x$ is a existing cell in the cluster. We can check if $x$ is close enough to affect growth by checking if

$$1 \leq |x - c| \leq 2. \tag{3.1}$$

Note that the first inequality should always hold. Let

$$\rho = |x - c|.$$

The intersection of the unit sphere at $c$ and the unit sphere at $x$ is a small circle, with axis $\vec{cx}$. Any point on the sphere within this small circle would be blocked from receiving growth. The vector $\vec{cx}$ can be written in spherical coordinates as

$$\rho = |x - c| = (\rho, \phi_A, \theta_A), \tag{3.2}$$

relative to the origin at point c. The center of the small circle is then $(1, \phi_A, \theta_A)$, and the angle of the cone of the small circle is $\omega = \arccos(\frac{\rho}{2})$. Let $T_A$ denote the linear

transformation that rotates the sphere so that the center of the small circle is moved to the north pole; that is,

$$T_A : (1, \phi_A, \theta_A) \rightarrow (1, 0, \theta_A). \tag{3.3}$$

Then the small disk on the sphere is given by the inequality $T_A(\phi) \leq \omega$. This inequality is of the form $f(\phi, \theta) \leq$ constant, or $g(u, v) \leq$ constant, after the change of coordinates

$$u = \cos\phi, \quad v = \theta. \tag{3.4}$$

Thus, for every neighboring cell in the cluster, we can determine a region on the sphere $S$ that is blocked for growth.

Once all blocked regions have been determined, it is time to select a spot for growth at random from the remaining open areas. We choose to describe points on the sphere using the transformed spherical coordinates $u = \cos\phi, v = \theta$. Then for each $v$ there will be corresponding values for $u$ where growth is blocked, and corresponding values for $u$ still open for growth. Clearly, if we first select a $v$, the selection of $v$ needs to be biased based on the density of open intervals of $u$'s still open for growth at $v$. To accomplish this we create a height function $h(v)$ defined as the total length of the segment [-1,1] that is still available. If there is no blocking at all at $v$, then $h(v) = 2$. If growth at $v$ is completely blocked, then $h(v) = 0$. The cell $c$ is declared dead if

$$h(v) \equiv 0 \text{ for all } v \in [0, 2\pi). \tag{3.5}$$

The integral

$$\int_0^{2\pi} h(v)\, dv \tag{3.6}$$

will then give the total area in the $u, v$ plane available for growth. For each $v$, assign a weighted probability $w(v)$ defined by

$$w(v) = \frac{h(v)}{\int_0^{2\pi} h(\alpha)\, d\alpha} \tag{3.7}$$

and then choose a value for $v$ based on those weighted probabilities. Note that if, for any $v$, $h(v) = 0$, then that $v$ will not be selected. Once a value for $v$ has been selected by this process, then for sure there is an open space for growth at $v$ at some value for $u \in [-1, 1]$, such that $g(u, v) \leq$ constant, as before.

The above method is sure-fire, in that once a existing cell is selected for new growth, all the blocked areas will be identified, and a location for new growth will be selected from the remaining open areas. A cell will be declared dead only if it's known for sure that all possible directions for growth are blocked. The problem with the above method is that it is very difficult to implement. Computing and storing the linear transformations $T$ and the height functions $h(v)$ for every neighboring cell is not feasible. So we must abandon the sure-fire approach in favor of a simpler, trial-and-error approach.

### 3.2.2 Random Direction Method

A random point $t$ on the sphere $S$ is selected by choosing $u \in [-1, 1]$ and $v \in [0, 2\pi)$. Then the point $t$ is tested to see whether it is blocked for growth by whether any existing cells of the cluster lie within a distance 1 from $t$. If not, new growth takes place at $t$. If it is blocked, then a new random $t$ is selected. This is repeated until either an unblocked direction for growth is found, or until a specified number of trials

has occurred and the current cell $c$ is declared dead. The algorithm is carried out for larger and larger values of this number of trials parameter, until asymptotic behavior is observed in the measured properties of the model.

Since new growth takes place at a random point that is a distance 1 away from the test node, an important process in the above model is selecting a random point on a sphere. Perhaps the most natural inclination is to describe the points on the unit sphere using the spherical coordinates

$$\rho = 1, \quad \phi \in [0, \pi], \quad \theta \in [0, 2\pi). \tag{3.8}$$

Randomly choosing an angle $\phi$ and then an angle $\theta$ will produce a point on the sphere, for sure, but since the $\phi$,$\theta$ grid is more concentrated near $\phi = 0$ and $\phi = \pi$, this method will favor growth at the poles.

In an attempt to counteract this, new coordinates of

$$u = \cos\phi, \quad v = \theta \tag{3.9}$$

are introduced. Now randomly choosing a $u \in [-1, 1]$ and $v \in [0, 2\pi)$ will no longer favor growth at the poles, since the transformation from the $u, v$ plane to the sphere is area-preserving.

### 3.2.3 Polyhedron Method

The process of selecting a site, or equivalently, a direction for new growth should ideally satisfy two criteria. First, the site should be chosen at random, and second, all possible sites, or directions, should be tried before giving up and declaring the test

cell to be dead. These two criteria conflict somewhat: it is possible that trying many random directions for growth will miss an entire region of possible growth.

The random direction method described in the previous section still does not produced *evenly − spaced* random points on the sphere, since an element of area in the $u, v$ plane mapped to the sphere will be elongated near the poles; i.e., the transformation is not length-preserving. This is an important consideration to ensure all possible directions for growth are tried; to make sure the tested directions are well spread-out, it would be best to randomly select from the vertices of a homogeneous grid of a sufficiently small size. Unfortunately, such a grid does not exist on the sphere [44].

However, the vertices of the five platonic solids, or regular convex polyhedra, are evenly-spaced, and lie on a sphere. The icosahedron has 12 such vertices, and the dodecahedron has 20. Since connecting the centers of the faces of an icosahedron creates a dodecahedron (and vice-versa), one can form an icosahedron-dodecahedron compound with 32 evenly-spaced vertices that lie on a single sphere. These 32 vertices can be randomly oriented by choosing an axis determined by a single point on the sphere, which can be randomly selected by using $u, v$ coordinates, as described above.

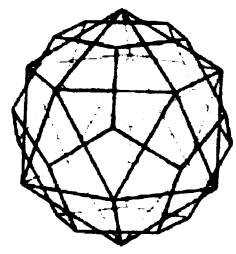

Figure 3.1: Icosahedron-dodecahedron compound.

This method will then produce 32 evenly- and regularly-spaced points on a sphere, but with a random orientation. One of these 32 points is selected to be the test location $t$. If growth is blocked, another of the 31 remaining points is selected. If all 32 points are blocked for growth, another 32 points can be generated by choosing another random orientation. This method seems to be a good compromise between the conflicting criteria of randomness and homogeneity.

## 3.3 Properties of the Model

Both numerical methods described above give similar results, with the polyhedron method showing a slightly faster convergence to equilibrium. The properties of the model discussed below do not depend on the method used.

### 3.3.1 Compactness

We relate the discrete Eden model to a continuous Markovian growth process, by re-defining time in the following way. At each time step $t$ growth takes place at each point on the boundary with probability $dt$. At time $t = 0$ only the seed at the origin is in the cluster, and at each time interval $dt$, an empty site on the surface of the cluster is added to the cluster with probability $dt$.

Recall that in the introduction, for the purposes of self-affine scaling, we defined time to be proportional to the radius of the cluster. Now we define time to be proportional to the surface area of the cluster. Naturally, for a three-dimensional cluster, radius and surface area are not proportional, so this is indeed a very different

definition of time. However, since time is not explicit in the model, we are free to define it as it is convenient.

Dhar [11] proves the compactness of Eden clusters using estimates that are lattice-dependent. The argument will now be shown to apply to off-lattice Eden clusters.

**Theorem 3** *Off-lattice Eden clusters grown in any dimension are compact; that is, they contain a negligible number of holes in the limit* $N \to \infty$.

The proof follows Dhar. First we show that $t_N$, the time for needed for the cluster to grow to size $N$, varies as $N^{\frac{1}{d}}$. This can be done by finding upper and lower bounds for $t_N$ that vary as $N^{\frac{1}{d}}$. The upper bound is obtained by Dhar using the lattice. Estimates will be obtained, first in two dimensions, and then in any dimension, for off-lattice clusters. It will be shown that the upper bound on $\langle t_N \rangle$ varies as $N^{\frac{1}{d}}$ for any dimension $d$.

Let $S_N$ be the total surface area available for new growth surrounding the cluster of size $N$ at time $t_N$. Then we have

$$\langle t_N \rangle = \int \frac{1}{S_N} dN. \tag{3.10}$$

For two-dimensional off-lattice clusters, $S_N$ represents the length of the boundary.

**Lemma 1** *In two dimensions,* $S_N \geq \pi + \frac{\pi}{3}(\sqrt{12N-3})$

**Proof** The lower bound for the surface area is given by the densest packing of circular cells. Note that in any dense packing (such as hexagonal close packing) adding a cell that touches two existing cells will increase the boundary by $\pi$, adding

a cell that touches 3 existing cells will increase the boundary by $\frac{2\pi}{3}$, adding a cell that touches 4 existing cells will increase the boundary by $\frac{\pi}{3}$, and adding a cell that touches 5 existing cells will not increase the boundary. As $N$ increases, it is seen that $S_N$ always exceeds $2\pi R$, where $R$ is the size of the hexagon that can be formed with a minimum of $N$ circles. Let $H_R$ be the number of circles in a hexagon of size $R$. By summing up finite series, it is easy to see that the relationship $N \geq H_R = 3R^2 - 3R + 1$ holds. Solving for $R$ gives the estimate for $S_N$.

□

**Lemma 2** *In two dimensions,* $\langle t_N \rangle < \frac{1}{2\pi}(12N-3)^{\frac{1}{2}} - \frac{3}{2\pi}$

**Proof** Substituting the estimate from Lemma 1 into $\langle t_N \rangle = \int \frac{1}{S_N} dN$, we get

$$\langle t_N \rangle \quad \leq \quad \frac{3}{\pi} \int \frac{1}{3 + \sqrt{12N-3}} dN \quad < \quad \frac{3}{\pi} \int \frac{1}{\sqrt{12N-3}} dN, \tag{3.11}$$

whereupon integrating and using that $t_1 = 0$ to get the constant of integration we have Lemma 2.

□

From Lemma 2 we see that in two dimensions, $\langle t_N \rangle$ varies at most as $N^{\frac{1}{2}}$. In three dimensions, the analogous formulas involved become much more complicated, so the details have been omitted.

**Lemma 3** *In d dimensions,* $S_N \geq f(N^{\frac{d-1}{d}}) \quad + \quad$ *lower order terms.*

**Proof** Generalize the argument in the proof of Lemma 1. Again, the lower bound for the surface area is given by a densest packing of spherical cells. For a

cluster of size $N$ spheres in a densest packing, we see as $N$ increases, $S_N$ always exceeds $R^{d-1}$, where $R$ is the size of the hexagonal hyper-solid that can be formed with a minimum of $N$ spheres. Then $N$ varies as $R^d$, or

$$R \sim N^{\frac{1}{d}},$$

so $S_N$ varies at least by $N^{\frac{d-1}{d}}$.

□

**Lemma 4** *In d dimensions,* $\langle t_N \rangle < dN^{\frac{1}{d}}$.

**Proof** Substitute the estimate from Lemma 3 into $\langle t_N \rangle = \int \frac{1}{S_N} dN$, and integrate as in Lemma 2.

$$\langle t_N \rangle \quad < \quad \int \frac{1}{N^{\frac{d-1}{d}}} dN \quad = \quad dN^{\frac{1}{d}}. \tag{3.12}$$

□

From Lemma 4 we see that $t_N$ varies at most as $N^{\frac{1}{d}}$. The rest of Dhar's argument is valid off-lattice: the average velocity $V$ with which the boundary moves outwards is bounded above by some $V_{\max}$, and $t_N$ is bounded below by $(d!N)^{\frac{1}{d}} 2V_{\max}$. Hence both the upper and lower bounds for $\langle t_N \rangle$ vary as $N^{\frac{1}{d}}$, and so the mean cluster size $V\langle t_N \rangle$ also must vary as $N^{\frac{1}{d}}$. So as $N$ gets large, the cluster has a negligible number of holes, and so off-lattice Eden clusters are compact in any dimension.

### 3.3.2 Density

Generating clusters of relatively small size (under $10^5$ cells), it appears that the algorithm does not produce clusters with constant density. Early in the growth process,

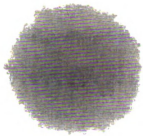

Figure 3.2: Typical Cluster of 100,000 cells.

the density steadily decreases as you move away from the center of mass. For a possible explanation, consider that in small clusters, the size of the cell is still large in relation to the size of the overall cluster, and so the surface of the cluster still has a significant local curvature. In this case, new growth can take place closer to the center of mass than the tangent plane to the cluster. For large clusters relative to the size of a single cell, the surface is locally nearly flat, and new growth can take place on or beyond the tangent plane to the cluster. So perhaps the density quickly levels off as the local curvature becomes insignificant.

To reduce the effects of the surface curvature, the algorithm was used to grow clusters inside a circular cylinder, and this significantly quickened the convergence to a constant density. However, the results stated below are based on eden clusters without any restrictions on growth.

Without any artificial limitations on the shape of the cluster, the algorithm grows clusters that are nearly spherical in shape, and after a mean radius of about 20 units,

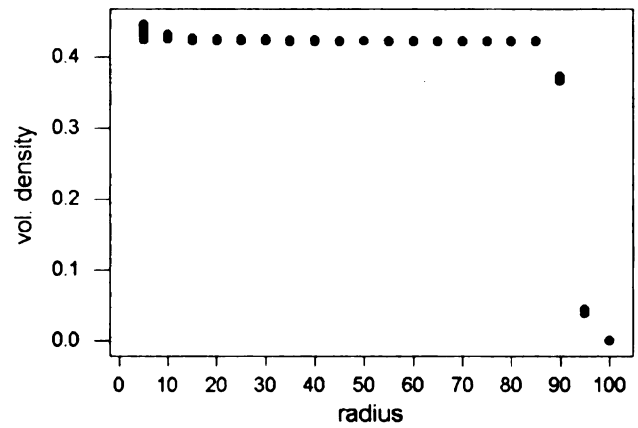


Figure 3.3: Typical graph of density versus radius. Radius is measured as distance from the center of mass. The above plot is of 15 simulations of a cluster of 2.5 million cells, using the random method with 1000 trials.

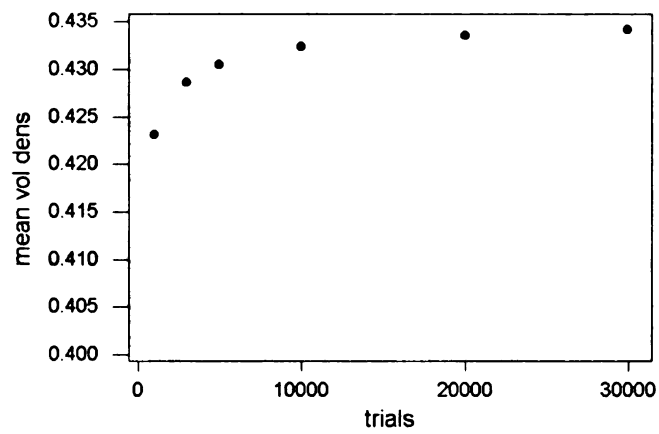


Figure 3.4: Graph of average density versus number of trials, using the random method, as shown in table 1.

the (volume) density is nearly constant at approximately 0.43. Here density is defined as the fraction of space occupied by the cells, if they were solid balls. For comparison, the density of closest packing of solid balls in three dimensions is 0.74.

The density of the clusters depends slightly on the number of trials, the parameter for how many times a new direction for growth is tried before a cell is declared dead. As expected, if the parameter trials is set low, cells may be given up for dead prematurely, and the density will be lower. Figure 3.4 shows the average volume density of clusters grown for different values of the trials parameter.

### 3.3.3 Scaling Properties: the Growth Exponent $\beta$

Since the algorithm is off-lattice, and thus isotropic, the Eden clusters generated have nearly spherical boundaries, but nonetheless rough. Next we look at the fractal-scaling growth exponent of the boundary. The surface width $\sigma$ is defined as the standard deviation of the radial distance from the center of mass for all surface sites; that is,

$$\sigma^2 = \frac{1}{N}\sum_{n=1}^{N}\{[(x_n - \bar{x})^2 + (y_n - \bar{y})^2 + (z_n - \bar{z})^2]^{\frac{1}{2}} - R\}^2, \tag{3.13}$$

where $N$ is the number of sites $(x_n, y_n, z_n)$ in the cluster's surface, and $R$ is the mean radius away from the center of mass $(\bar{x}, \bar{y}, \bar{z})$. Then the surface-width scaling exponent $\beta$, defined by

$$\sigma \sim R^{\beta}, \tag{3.14}$$

is determined to be approximately 0.12. For the results of several simulations, please see the table at the end of this section. This indicates that the growth exponent

scaling of the off-lattice Eden model in the radial geometry is consistent with the small-slope regime present in the continuum equation.

The surface-width scaling growth exponent $\beta$ is calculated in the following way. As a cluster is grown, the surface width $\sigma$ and mean radius $R$ is calculated at regular intervals. Then a linear regression of $\log(\sigma)$ against $\log(R)$ yields the exponent $\beta$ as the slope of the regression line. The reported value for $\beta$ is the average of many simulations (typically about 15). This can be done in several ways: (a) compute $\beta$ for each simulation, then find the average; (b) first average the values for surface width $\sigma$ and mean radius $R$ over all simulations, then compute $\beta$ by regressing the averages; and (c) run the regression using the values for $\sigma$ and $R$ from all the simulations pooled together. All three methods yield nearly identical results. Following are typical regression plots illustrating methods (b) and (c), and the page after that shows the results of several simulations of both the random direction and polyhedron methods. The confidence intervals stated in those tables are based on regression method (c).

| Simulation Results for Estimating Beta: Random Method | | | | |
|---|---|---|---|---|
| Trials | Size of Cluster | Simulations | Density | Beta |
| 1000 | 2.5 million | 15 | 0.80824 | 0.137 +/- 0.014 |
| 3000 | 2.5 million | 15 | 0.81870 | 0.129 +/- 0.012 |
| 5000 | 2.5 million | 15 | 0.82223 | 0.123 +/- 0.015 |
| 10000 | 2.5 million | 15 | 0.82587 | 0.120 +/- 0.013 |

Table 3.1: Simulation Results for Estimating Beta: Random Method

| Simulation Results for Estimating Beta: Polyhedron Method | | | | |
|---|---|---|---|---|
| Trials | Size of Cluster | Simulations | Density | Beta |
| 30*32 = 960 | 2.5 million | 15 | 0.80405 | 0.137 +/- 0.011 |
| 100*32=3200 | 2.5 million | 15 | 0.81554 | 0.113 +/- 0.010 |
| 150*32=4800 | 2.5 million | 15 | 0.81849 | 0.121 +/- 0.015 |
| 300*32=9600 | 2.5 million | 15 | 0.82195 | 0.119 +/- 0.011 |
| 500*32=16000 | 2.5 million | 13 | 0.82407 | 0.117+/- 0.014 |

Table 3.2: Simulation Results for Estimating Beta: Polyhedron Method

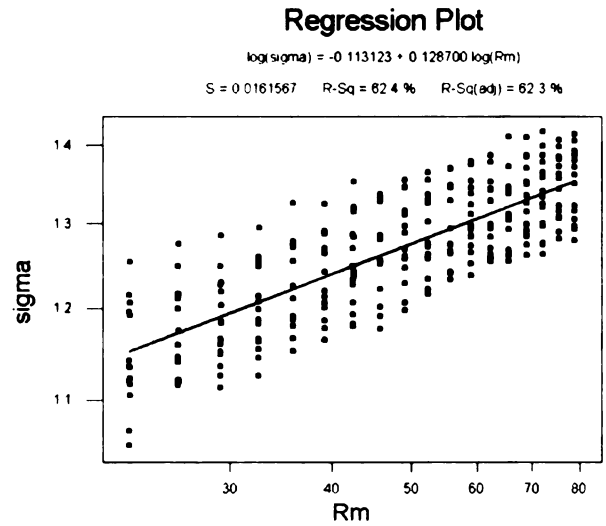


Figure 3.5: Regression using method (c). $\sigma$ and $R$ for all simulations are plotted on the same logarithmic scale and $\beta$ is the slope of the regression line.

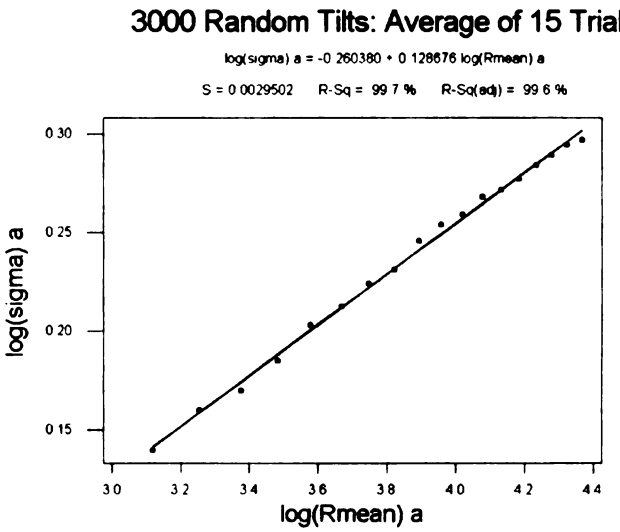


Figure 3.6: Regression using method (b). $\sigma$ and $R$ for all simulations are first averaged, then the average values are plotted on a logarithmic scale.

# Chapter 4

# Conclusion

In the physically important case $d = 2$ for surfaces grown in three dimensions, previous analytical and numerical investigations of the KPZ equation for the growth of rough surfaces have been inconclusive. A new stochastic differential equation is proposed to study $d = 2$ surface propagation in a three-dimensional radial geometry, and a new discrete model for three-dimensional off-lattice Eden surface growth in a radial geometry is implemented.

Like the KPZ equation, the radial growth equation presented in Chapter 2 incorporates lateral growth, surface tension, and random noise. For $d = 1$, the radial equation with a noise term of $\pm R^{-1/2}$ grows surfaces with growth exponent $\beta \approx \frac{1}{3}$, which is consistent with the well-understood $d = 1$ case for the KPZ equation, and consistent with previous Eden cluster simulations using both flat and radial geometries, and both on and off a lattice. This confirms that the scaling behavior in this dimension is quite stable, and off-lattice radial Eden cluster growth, and indeed perhaps all kinds of Eden growth belongs to the $d = 1$ KPZ universality class.

For higher dimensions, this stability is not present. Numerical investigation of the radial growth equation for the case $d = 2$ exhibits two distinct scaling regimes. For early times, there is a small-$\beta$ regime, where $\beta$ is consistently found to be approximately 0.12. Then there is a crossover to a large-$\beta$ regime, where $\beta$ is consistently

found to be approximately 0.22. The crossover appears to be strongly effected by the coupling of the velocity $v$ and the surface tension $\nu$. Both small-$\beta$ and large-$\beta$ results have been found in previous numerical investigations of the KPZ equations. However most, including all of the recent studies, report a value consistent with the large-$\beta$ regime. A crossover between two scaling regimes for the growth exponent $\beta$ is not known to have been reported in any previous study of the KPZ equation.

It was shown in Chapter 2 that the radial equation reduces to the KPZ equation in the large-radius limit as expected. In the numerical simulations, it was observed that for large $R$, the scaling behavior crossed over to a regime where the growth exponent $\beta$ is consistent with several recent numerical and analytical studies of the KPZ equation [7, 9, 31].

The discrete model discussed in Chapter 3 is an off-lattice version of Eden cluster growth in the radial geometry. The model grows compact clusters with constant density for large clusters. Here the growth exponent for the surface of the clusters is found to be approximately 0.12, consistent with the small-$\beta$ regime of the radial equation, and no crossover behavior is observed. It may be that in the discrete model, as opposed to the continuous case, the surface tension remains significant throughout the growth process, even for large clusters.

The question of placing three-dimensional Eden cluster growth in the universality class of a continuum equation is thus a complicated one, since the scaling behavior of both the KPZ equation and the radial equation is uncertain. If indeed $\beta \approx 0.22$ for the $d = 2$ KPZ equation, then it is found that the off-lattice Eden cluster model in the radial geometry does not belong to the KPZ universality class. It is conjectured

that the radial geometry has a strong effect on the growth exponent. The large-$\beta$ regime occurs when the growth velocity dominates the surface tension. Kardar, Parisi and Zhang suggested that this behavior is to be expected for Eden growth, as surface tension is not expected to be influential [23]. However, off-lattice Eden growth in the radial geometry could be expected to exhibit a much stronger surface tension, as growth is now permitted much closer to the center of mass. It is proposed that the additional surface tension exhibited in the off-lattice radial geometry is sufficient to keep the scaling behavior in the small-$\beta$ regime.

There has been recent concern over the discretizations used in the numerical analysis of the KPZ equation [28, 29, 30]. Honda and Matsuyama [19] argue that the large $\beta$ frequently found for the KPZ equation for $d = 2$ is due to the discretization of the equation, in both analytical and numerical studies. If the effect of the discretization is significant, then this effect would be present in numerical results in this paper as well.

A more careful and detail numerical study of the radial growth equation thus could prove to be beneficial. An improved discretization technique would allow for growth to be simulated over larger times to investigate the large-radius behavior. Similarly further analysis of the surface tension dominated weak-coupling regime that appears to govern the small-$\beta$ scaling regime exhibited by the radial equation and the off-lattice radial Eden cluster is needed. The crossover phenomenon should be investigated further to understand the relationship between the crossover time and the coupling of the velocity and surface tension. Lastly, a theoretical analysis of the relationship between random noise in the flat and radial geometries in three

dimensions is desired to better understand the radial continuum equation and its relationship with the KPZ equation.

# BIBLIOGRAPHY


[1] Appert C, 'Large Deviation Function for the Eden Model and Universality within the One-dimensional Kardar-Parisi-Zhang Class,' *Phys. Rev. E* 61 (2) 2092 (2000).

[2] Baish J and Jain R, 'Fractals and Cancer,'*Cancer Research* 60 3683 (2000).

[3] Barabási A L and Stanley H E, *Fractal Concepts in Surface Growth* (Cambridge University Press) (1995).

[4] Batchelor M T, Henry B I, 'Limits to Eden Growth in Two and Three Dimensions,' *Physics Letters A* 157 (4,5) 229 (1991).

[5] Batchelor MT, Henry B I and Watt S D, 'Continuum Model for Radial Surface Growth,'*Physica A* 260 11 (1998).

[6] Beccaria M and Curci G, 'Numerical Simulation of the Kardar-Parisi-Zhang Equation,' *Phys. Rev. E* 50 (6) 4560 (1994).

[7] Castellano C, Gabrielli A, Marsili M, Muñoz M A and Pietronero L, 'High Dimensional Behavior of the Kardar-Parisi-Zhang Growth Dynamics,' *Phys. Rev. E* 58 (5) R5209 (1998).

[8] Chakrabarti A and Toral R, 'Numerical Study of a Model for Interface Growth,' *Phys. Rev. B* 40 (16) 11419 (1989).

[9] Colaiori F and Moore M A, 'Stretched Exponential Relaxation in the Mode-coupling Theory for the Kardar-Parisi-Zhang Equation,' *Phys. Rev. A* 63 057103-1 (2001).

[10] Colairori F and Moore M A, 'Upper Critical Dimension, Dynamic Exponent, and Scaling Functions in the Mode-coupling Theory for the Kardar-Parisi-Zhang Equation,' *Phys. Rev. Lett.* 86 (18) 3946 (2001).

[11] Dhar D, 'Comment on "Eden Model in Many Dimensions",'*Physical Review Letters* 54 (18) 2058 (1985).

[12] Devillard P and Stanley H E, 'Scaling Properties of Eden Clusters in Three and Four Dimensions,' *Physica A* 160 298 (1989).

[13] Eden M,*Proc. 4th Berkeley Symp. Math. Stat. Prob.* 33 (1961).

[14] Family F and Vicsek T, 'Scaling of the Active Zone in the Eden Process on Percolation Networks and the Ballistic Deposition Model,' *J. Phys. A* 18 L75 (1985).

[15] Freche P, Stauffer D and Stanley H E, 'Surface Structure and Anisotropy of Eden Clusters,' *J. Phys. A: Math. Gen.* 18 L1163 (1985).

[16] Guo H, Grossman B and Grant M, 'Kinetics of Interface Growth in Driven Systems,' *Phys. Rev. Lett.* 64 (11) 1262 (1990).

[17] Halpin-Healy T and Zhang Y C, 'Kinetic Roughening Phenomena, Stochastic Growth, Directed Polymers and all that. Aspects of Multidisciplinary Statistical Mechanics,'*Phys. Rep.* 254 215 (1995).

[18] Hirsch R and Wolf D E, 'Anisotropy and Scaling of Eden Clusters in Two and Three Dimensions,' *J. Phys. A: Math. Gen.* 19 L251 (1986).

[19] Honda K and Matsuyama T J, 'Smooth Surface Solutions of the Kardar-Parisi-Zhang Equation in Dimensions Higher than 2 + 1,' *Phys. Soc. Japan* 68 (10) 3236 (1999).

[20] Julien R and Botet R, 'Scaling Properties of the Surface of the Eden Model in $d = 2, 3, 4$,' *J. Phys. A* 18 2279 (1985).

[21] Julien R and Botet R, *Fractals in Physics* ed L Pietronero and E Tosatti (Amsterdam:Elsevier) p 251 (1986).

[22] Kardar M, Parisi G. and Zhang Y C, 'Dynamic Scaling of Growing Interfaces,' *Phys. Rev. Lett.* 56 (9) 889 (1986).

[23] Kardar M, Parisi G. and Zhang Y C, 'Kardar, Parisi, and Zhang Respond,' *Phys. Rev. Lett.* 57 (14) 1810 (1986).

[24] Keblinski P, Maritan A, Toigo F, Messier R and Banavar J,'Continuum Model for the Growth of Interfaces,' *Phys. Rev. E* 53 (1) 759 (1996).

[25] Kertész J and Wolf D, 'Noise Reduction in Eden Models: II. Surface Structure and Intrinsic Width,' *J. Phys. A: Math. Gen.* 21 747 (1988).

[26] Kertész J and Wolf D, 'Growth of Self-affine Surfaces,' *Physica D* 38 221 (1989).

[27] Kim J M and Kosterlitz J M, 'Growth in a Restricted Solid-on-Solid Model,' *Phys. Rev. Lett.* (19) 2289 (1989).

[28] Ko D Y K and Seno F, 'Simulations of Deposition Growth Models in Various Dimensions: The Possible Importance of Overhangs,'*Phys. Rev. E* 50 (3) R1741 (1994).

[29] Lam C H and Shin F G, 'Anomaly in Numerical Integrations of the Kardar-Parisi-Zhang Equation,' *Phys. Rev. E* 57 (6) 6506 (1998).

[30] Lam C H and Shin F G, 'Improved Discretization of the Kardar-Parisi-Zhang Equation,' *Phys. Rev. E* 58 (5) 5592 (1998).

[31] Marinari E, Pagnani A and Parisi G, 'Critical Exponents of the KPZ Equation via Multi-surface Coding Numerical Simulations,' *J. Phys. A: Math. Gen.* 33 8181 (2000).

[32] Marsili M, Maritan A, Toigo F and Banavar J R, 'Stochastic Growth Equations and Reparameterization Invariance,'*Rev. Mod. Phys.* 68 (4) 963 (1996).

[33] Meakin P, Jullien R and Botet R, 'Large-scale Numerical Investigation of the Surface of Eden Clusters,' *Europhys. Lett.* 1 (12) 609 (1986).

[34] Meakin P, 'Noise-reduced and Anisotropy-enhanced Eden and Screened-growth Models,' *Phy. Rev. A* 38 (1) 418 (1988).

[35] Medina E, Hwa T and Kardar M and Zhang Y C, 'Burgers Equation with Correlated Noise: Renormalization-group Analysis and Applications to Directed Polymers and Interface Growth,' *Phys. Rev. A* 39 (6) 3053 (1989).

[36] Moser K, Kertsz J and Wolf D E, 'Numerical Solution of the Kardar-Parisi-Zhang Equation in One, Two and Three Dimensions,' *Physica A* 178 215 (1991).

[37] Plischke M and Rácz Z, 'Active Zone of Growing Clusters: Diffusion-limited Aggregation and the Eden Model,' *Phys. Rev. Lett.* 53 (5) 415 (1984).

[38] Plischke M and Rácz Z, 'Dynamic Scaling and the Surface Structure of Eden Clusters,' *Phys. Rev. A* 32 (6) 3825 (1985).

[39] Rácz Z and Plischke M, 'Active Zone of Growing Clusters: Diffusion-limited Aggregation and the Eden Model in Two and Three Dimensions,' *Phys. Rev. A* 31 (2) 985 (1985).

[40] Stauffer D, 'Cumulant Ratios of Eden Surfaces in 1+1 Dimensions,' *Int. J. Mod. Phys.* 9 (7) 1033 (1998).

[41] Vicsek T, *Fractal Growth Phenomena* (World Scientific:Singapore)(1992).

[42] Weichsel I, 'Dynamics of Eden Clusters: Confirmation of Appert-Derrida Universality,' *Int. J. Mod. Phys.* 11 (4) 691 (2000).

[43] Wang C Y, Liu P L and Bassingthwaighte J B, 'Off-lattice Eden-C Cluster Growth Model,' *J. Phys. A: Math. Gen.* 28 2141 (1995).

[44] Wang C Y, and Bassingthwaighte J B, 'Biological Growth on a Surface,' *Math. Biosci.* 142 91 (1997).

[45] Wolf D E, 'Wulff Construction and Anisotropic Surface Properties of Two-dimensional Eden Clusters,' *J. Phys. A: Math. Gen.* 20 1251 (1987).

[46] Wolf D E and Kertsz J, 'Surface Width Exponents for Three- and Four-dimensional Eden Growth,' *Europhys. Lett.* 4 (6) 651 (1987).

[47] Zabolitzsky J G and Stauffer D, 'Simulation of Large Eden Clusters,' *Phys. Rev. A* 34 (2) 1523 (1986).